CHAPTER 4

SATURATED FLOW BOILING OF FC-72 ON A HEADED MICRO PIN-FINNED SILICON CHIP FLUSH MOUNTED ON BOTTOM OF RECTANGULAR CHANNEL

The results obtained in the first part of the study are presented in this chapter to illustrate the saturated flow boiling heat transfer on a heated micro pin-finned silicon chip flush mounted onto the bottom of a rectangular channel. The present experiments are carried out for the coolant FC-72 flowing in a rectangular channel with the mass flux varying from 287 kg/m^{2}s to 431 kg/m^{2}s, and imposed heat flux from 0.1 W/cm^2 to 10 W/cm^2. Besides, the silicon chips contain three different surface micro-structures, namely, the smooth, pin-finned 200 and pin-finned 100 surfaces. The coolant is at atmospheric pressure with T_{sat} = 54.3 ^{o}C.

In the following, effects of the coolant mass flux, imposed heat flux, and surface micro-structures on the saturated flow boiling heat transfer performance and associated bubble characteristics will be examined in detail. The heat transfer performance is presented in terms of the boiling curves and boiling heat transfer coefficients.

4.1 Single-phase Liquid Convective Heat Transfer

Before beginning the two-phase flow boiling experiments, the single-phase convective heat transfer experiments are conducted for liquid FC-72. The measured single-phase convection heat transfer coefficients for the chip with a smooth surface are compared with the correlation proposed by Gersey and Mudawar [7]. The correlation of Gersey and Mudawar [7] is

$$\overline{Nu}_L = 0.362 \cdot Re_L^{0.614} \cdot Pr^{1/3} \tag{4.1}$$

where

$$Re_L = \frac{G \cdot L}{\mu_l} \tag{4.2}$$

$$\bar{h}_{1\phi} = \frac{k_l}{L} \cdot \overline{Nu}_L \tag{4.3}$$

for the flow velocity ranging from 13 cm/s to 400 cm/s

Their correlation is based on the experimental data procured from the same liquid and same flow configuration as the present data and the comparison is shown in Fig. 4.1 for the dimensional and dimensionless heat transfer coefficients. The results indicate that our data are in good agreements with their correlation. Then the present data for the chips with pin-finned surface are given in Fig. 4.2. Note that a significant enhancement in the liquid convection heat transfer can be obtained by adding the micro pin-fins to the chip surface. The enhancement is more pronounced at a higher flow rate (Reynolds number). Besides, the chip surface with the smaller and denser fins shows a better heat transfer performance. The measured data for the pin-finned surface can be correlated as

$$\overline{Nu}_L = 0.33 \cdot Re_L^{0.64} \cdot Pr^{1/3} \cdot F_{sp} \tag{4.4}$$

with the factor F_{sp} accounting for the geometry effects of the fins and it can be correlated as

$$F_{sp} = \left(\frac{S_f}{H}\right)^{-0.15} \left(\frac{H\text{-}B_f}{W_f}\right)^{-0.06} \left(\frac{NA_f}{A_s}\right)^{0.04} \tag{4.5}$$

Here S_f is the fin space between two adjacent fins, H is the rectangular channel height, B_f is the fin height, W_f is the fin width, N is the total number of pin-fins, A_f is the surface area of a single fin, and A_s is the surface area of the bare chip.

It should be mentioned that all of the working fluid properties used in reducing the data for Figs. 4.1 and 4.2 and Equations 4.1 - 4.4 are calculated at the coolant inlet

temperature. The chip length is chosen as the characteristic length for the Reynolds number Re_L and average Nusselt number $\overline{Nu}_L$ because of its significant effect on the heat transfer performance.

4.2 Saturated Flow Boiling Curves

The effects of the coolant mass flux G and surface micro-structures of the heated silicon chip on the boiling curves in the saturated boiling flow are shown in Figs. 4.3 - 4.6. Figure 4.3(a) shows the effects of the mass flux on boiling curves for the chip with smooth surface. Note that for a given G the temperature of the chip surface increases gradually with the imposed heat flux at a low q from the saturated temperature of the coolant to a certain value just exceeding T_{sat} and no bubble nucleation is observed. The heat transfer in this region is completely due to the single-phase forced convection. With the continuing increase in the surface heat flux, bubbles begin to appear on the surface and the boiling curve is characterized by a sharp increase in the surface heat flux for a small rise in the temperature of chip surface. We have onset of nucleate boiling (ONB) in the flow. The reason causing the transition on the boiling curve is due to a significant increase in the surface heat transfer by the boiling processes. Note that beyond ONB the coolant mass flux has slight effects on the boiling curves, suggesting that the surface heat transfer is mainly dominated by the fully developed nucleate boiling. Besides, at a higher G the required heat flux for ONB is higher and this implies that more energy is needed for the vapor to nucleate from the wall since the residence time of the coolant on the chip is shorter. Checking the results in Figs. 4.3(b) and (c) reveal that for the pin-finned surfaces the boiling curves show similar trends to that for the smooth surface.

Then, how the boiling curve is affected by the surface micro-structure of the chip is

shown in Fig. 4.4. The results clearly indicate that in both the single-phase and nucleate boiling regions at the same wall superheat the chip surface heat flux is highest for the pin-finned 100 surface and lowest for the smooth surface, suggesting that using the micro pin-finned structure can effectively enhance the single-phase and flow boiling heat transfer from the chip surface. The large increase in the total surface area by the micro pin-fins is indeed beneficial for the single- and two-phase heat transfer. Besides, the wall superheat required for the boiling inception is substantially lower for the pin-finned 100 surface. This is attributed to the increase in the density of the active nucleation sites by the surface micro-structures. Particularly, in the corner region of the pin fins the bubbles are found to appear at a lower ΔT_{sat}.

4.3 Saturated Flow Boiling Heat Transfer Coefficient

We continue to explore how the saturated flow boiling heat transfer coefficient $h_{2\phi,sat}$ is affected by the FC-72 coolant mass flux and the surface micro-structures on the silicon chips. The results for the variations of $h_{2\phi,sat}$ with the surface heat flux presented in Figs. 4.5 and 4.6 reveal that for smooth and finned surfaces the coolant mass flux shows negligible influences on the flow boiling heat transfer coefficients. However, for a given coolant mass flux the boiling heat transfer coefficient increases substantially with the imposed heat flux.

Finally, it is noted from Fig. 4.6 that adding the surface micro-structures in the form of micro-pin-fins to the silicon chip produces some positive effects on the boiling heat transfer coefficient at high imposed heat flux. This is due to the fact that the boiling heat transfer performance can be raised effectively by the addition of active nucleation sites from the pin-fin structures. Besides, the heat transfer is further enhanced by a serpentine motion of liquid between adjacent rows of pin-fins, which in

turn enhance turbulent mixing. Furthermore, development of multiple thermal entry regions at the top surfaces of individual pin-fins is beneficial.

4.4 Bubble characteristics

To elucidate the saturated flow boiling heat transfer characteristics, the data for the bubble characteristics obtained from the present flow visualization are examined in the following. At first, the top views of the boiling flow for various coolant mass flow rates and imposed heat fluxes are shown in Figs. 4.7 - 4.9 for the smooth and micro-structured surfaces. The vapor bubbles begin to appear as the chip surface temperature exceeds the boiling incipient superheat. In the beginning, tiny bubbles are obviously observed in the active nucleation sites. The bubbles grow and then detach from the chip surface with certain mean bubble departure diameters. As the imposed heat flux increases, more bubbles are generated on more active nucleation sites and more bubbles detach from the chip surface. Besides, the detached bubbles tend to merge into larger bubbles. Note that the large bubbles become distorted and elongated as they slide on the heating surface. To quantify the bubble characteristics, the measured data for the mean bubble departure diameter and frequency and active nucleation site density are given in Figs. 4.10 - 4.15 showing the effects of the coolant mass flux, imposed heat flux, and surface micro-structure.

The results in Fig. 4.10 obviously indicate that the mean size of the bubbles departing from the chips with the smooth and finned surfaces can be reduced substantially by increasing the coolant mass flux. It reflects the fact that the coolant at a higher mass flux and hence at a higher speed tends to sweep the bubbles more quickly away from the heating surface. Besides, the addition of the micro pin-fins to the chips causes a significantly earlier departure of the bubbles from the chip surfaces and results in a smaller bubble departure diameter (Fig. 4.11). The partially

accelerated coolant flow between the fins can effectively enhance the drag force on the bubbles and sweep the bubbles away from the finned surface earlier. Note that the mean bubble departure diameter for the pin-finned 100 surface is larger than that for the pin-finned 200 surface. This due to the fact that the spaces between the adjacent fins for the pin-finned 100 surface are so small and the bubbles already contact the sides of the fins before departure. Therefore, the bubbles grow for a longer period of time before they detach from the chip surface. Longer bubble growth time causes the growing bubble to keep absorbing energy from the heated surface and results in a larger mean bubble departure diameter.

Next, the data given in Fig. 4.12 manifest that raising the coolant mass flux can significantly augment the mean bubble departure frequency. The increase of f with G is ascribed again to the higher drag on the bubbles still attaching to the chip surface by the liquid coolant moving at a higher speed for a higher G. This, in turn, causes an earlier departure of the bubbles from the surface, resulting in a higher departure frequency. It is also observed that the mean bubble departure frequency increases noticeably with the imposed heat flux. Finally, the data given in Fig. 4.13 indicate that the bubble departure frequency can be enhanced effectively by using the pin-finned surface and the phenomenon is more pronounced on the pin-finned 200 surface than that on the pin-finned 100 surface.

Attention is turned to the data for the mean active nucleation site density shown in Figs. 4.14 and 4.15. The active nucleation site density is calculated based on the surface area of a bare chip. Figure 4.14 manifests that an increase in the coolant mass flux results in somewhat lower active nucleation site densities for the smooth and micro-structured surfaces. This directly relates to the higher imposed heat flux is needed for the boiling inception at a higher G, as already discussed in the previous section. Finally, it is noted from Fig. 4.15 that adding the micro pin-fins to the chip

surface can effectively increase the active nucleation sites. This is due to the addition of the surface area of micro pin-fins. More specifically, the nucleation site density on the pin-finned 100 surface is slightly higher than that on the pin-finned 200 surface.

4.5 Correlation Equations

According to the present experimental data, empirical correlations for the heat transfer coefficient in the saturated flow boiling of FC-72 on the heated silicon chip flush mounted on the bottom of the rectangular channel is proposed here. The correlating equations for the smooth and micro pin-finned surfaces are respectively

$$Nu_{2\phi,sat} = \frac{h_{2\phi,sat} \cdot L}{k_l} = [80 \cdot Fr_l^{0.8} + 150 \cdot Bo^{0.4} \cdot Ja^{1.2}] \quad (4.6)$$

and

$$Nu_{2\phi,sat} = \frac{h_{2\phi,sat} \cdot L}{k_l} = [85 \cdot Fr_l^{0.7} + 210 \cdot Bo^{0.38} \cdot Ja^{1.02} \cdot F_{tp,sat}] \quad (4.7)$$

Here the Froude number Fr_l, Boiling number Bo and Jacob number Ja are respectively defined as

$$Fr_l = \frac{G^2}{\rho_l^2 \cdot g \cdot D_h} \quad (4.8)$$

$$Bo = \frac{q''}{G \cdot i_{lv}} \quad (4.9)$$

and

$$Ja = \frac{\rho_l \cdot C_{pl} \cdot \Delta T_{sat}}{\rho_v \cdot i_{lv}} \quad (4.10)$$

where G is the coolant mass flux, ρ_l is the liquid density, g is the acceleration due to gravity, D_h is the hydraulic diameter of the test section, c_{pl} is the liquid specific heat, $\Delta T_{sat} = T_w - T_{sat}$ is the wall superheat, and L is the chip length. Besides, a dimensionless factor $F_{tp,sat}$ is used to account for the effect of the geometric arrangements of the micro-pin-fins on the boiling heat transfer coefficient and it is defined as

$$F_{tp,sat} = \left(\frac{S_f}{H}\right)^{-0.2}\left(\frac{H-B_f}{W_f}\right)^{-0.06}\left(\frac{N\cdot A_f}{A_s}\right)^{0.4} \quad (4.11)$$

where S_f is the space between two adjacent fins, H is the rectangular channel height, B_f is the fin height, W_f is the fin width, N is the total number of pin-fins on a chip, A_f is the total surface area of a single fin, and A_s is the surface area of a bare chip. The proposed correlations are compared with the present data in Figs. 4.16 and 4.17. The comparison indicates that our data can be correlated with a deviation less than $\pm 25\%$ by the above empirical equations.

Then, empirical correlations for the average bubble departure diameter in FC-72 saturated flow boiling on the heated silicon chip flush mounted on the bottom of the rectangular channel estimated from the present flow visualization are proposed as

$$\frac{d_p}{\sqrt{\sigma/g\cdot\Delta\rho}} = \frac{0.25\cdot(\rho_l/\rho_v)^{0.48}\cdot Bo^{0.21}}{Re_l^{0.08}} \quad \text{for smooth surafce,} \quad (4.12)$$

and

$$\frac{d_p}{\sqrt{\sigma/g\cdot\Delta\rho}} = \frac{0.15\cdot(\rho_l/\rho_v)^{0.46}\cdot Bo^{0.24}\cdot F_{d,sat}}{Re_l^{0.07}} \quad \text{for pin-finned surfaces} \quad (4.13)$$

with the fin-geometry factor $F_{d,sat}$ correlated as

$$F_{d,sat} = \left(\frac{S_f}{H}\right)^{-0.12}\left(\frac{H-B_f}{W_f}\right)^{0.05}\left(\frac{N\cdot A_f}{A_s}\right)^{0.42} \quad (4.14)$$

Here Re_l is the all liquid Reynolds number based on the chip length and it is defined as

$$Re_l = \frac{G\cdot L}{\mu_l} \quad (4.15)$$

Note that $F_{d,sat}$ is a dimensionless factor to account for the fin-geometry effects on the mean bubble departure diameter. Figures 4.18 and 4.19 show that the present experimental data fall within ± 20 % of the correlations given in Equations (4.12) and (4.13). In addition, empirical equations are provided to correlate the data for the mean bubble departure frequency as

$$\frac{f \cdot d_p}{\mu_l/\rho_l \cdot D_h} = 0.65 Re_l^{1.3} \cdot Pr^{0.7} \cdot Bo^{0.66} \quad \text{for smooth surface,} \tag{4.16}$$

and

$$\frac{f \cdot d_p}{\mu_l/\rho_l \cdot D_h} = 0.21 Re_l^{1.3} \cdot Pr^{0.72} \cdot Bo^{0.66} \cdot F_{fin,sat} \quad \text{for pin-finned surfaces} \tag{4.17}$$

with the fin-geometry factor $F_{fin,sat}$

$$F_{fin,sat} = \left(\frac{S_f}{H}\right)^{0.12} \left(\frac{H\text{-}B_f}{W_f}\right)^{0.4} \left(\frac{N \cdot A_f}{A_s}\right)^{-0.02} \tag{4.18}$$

where $F_{fin,sat}$ is a dimensionless factor accounting for fin-geometry effects on mean bubble departure frequency. Figures 4.20 and 4.21 reveal that the present experimental data for $f \cdot d_p$ can be correlated with the deviation less than ± 25 % by the above two equations. Moreover, empirical correlations for the mean active nucleation site density in the FC-72 saturated flow boiling deduced from the present flow visualization are proposed as

$$N_{ac} \cdot d_p^{\,2} = 75 \cdot Bo^{0.84} \cdot Re_l^{-0.15} \quad \text{for smooth surface,} \tag{4.19}$$

and

$$N_{ac} \cdot d_p^{\,2} = 72 \cdot Bo^{0.87} \cdot Re_l^{-0.15} \cdot F_{n,sat} \quad \text{for pin-finned surfaces} \tag{4.20}$$

with the factor $F_{n,sat}$ correlated as

$$F_{n,sat} = \left(\frac{S_f}{H}\right)^{-0.15} \left(\frac{H\text{-}B_f}{W_f}\right)^{-0.06} \left(\frac{N \cdot A_f}{A_s}\right)^{1.15} \tag{4.21}$$

where $F_{n,sat}$ is a dimensionless factor to include the fin geometry effects on the active nucleation site density. The comparison in Figs. 4.22 and 4.23 show that more than 85 % of the present experimental data fall within ± 30 % of the correlation given in Equations (4.19) and (4.20).

Finally, the total heat flux input to the boiling flow q_t'' is considered to be composed of two parts: one resulting from the bubble nucleation q_b'' and another due to the single phase forced convection q_c''. Thus

$$q_t'' = q_b'' + q_c'' \tag{4.22}$$

Here q_b'' can be calculated from the quantitative data for the bubble characteristics examined in section 4.4 as

$$q_b'' = \rho_v \cdot V_v \cdot f \cdot N_{ac} \cdot i_{lv} \tag{4.23}$$

where ρ_v is the vapor density, V_v is the volume of the departing bubble defined as $\frac{4\pi}{3}(\frac{d_p}{2})^3$, f is the bubble departure frequency, N_{ac} is the active nucleation site density, and i_{lv} is the enthalpy of vaporization. Besides, q_c'' can be estimated from the single-phase liquid convection as

$$q_c'' = E \cdot \bar{h}_{1\phi} \cdot \Delta T_{sat} \tag{4.24}$$

where E is an enhancement factor added to account for the agitating motion of the bubbles which can enhance the single phase heat transfer. From the experimental data, E can be empirically correlated as

$$E = 4.5 \cdot N_{conf}{}^{0.5} \cdot Fr_l^{0.15} \cdot (1 + 280 \cdot Bo)^{1.8} \quad \text{for smooth surface,} \tag{4.25}$$

and

$$E = 2.8 \cdot N_{conf}{}^{0.5} \cdot Fr_l^{0.13} \cdot (1 + 270 \cdot Bo)^{1.8} \cdot F_{E,sat} \quad \text{for pin-finned surfaces} \tag{4.26}$$

with the fin-geometry factor $F_{E,sat}$

$$F_{E,sat} = (\frac{S_f}{H})^{-0.16} (\frac{H\text{-}B_f}{W_f})^{-0.1} (\frac{N \cdot A_f}{A_s})^{0.02} \tag{4.27}$$

where $F_{E,sat}$ accounts for the fin-geometry effects on the enhancement factor. The dimensionless factor N_{conf} is the Confinement number and it is defined as

$$N_{conf} = \frac{(\sigma/g \cdot \Delta\rho)^{0.5}}{D_h} \tag{4.28}$$

The results in Figs. 4.24 & 4.25 indicate that the experimental measured data can be correlated with the deviation less than $\pm 25\%$ by the present empirical correlation given in eq. (4.22).

4.6 Concluding Remarks

An experimental study has been carried out to investigate FC-72 saturated flow boiling heat transfer performance and associated bubble characteristics on a heated micro-pin-finned silicon chip flush mounted on the bottom of a rectangular channel. The effects of the imposed heat flux, coolant mass flux and geometry of the surface micro-structures on the saturated flow boiling heat transfer coefficients and the associated bubble characteristics such as the mean bubble departure diameter, bubble departure frequency, and active nucleation site density have been examined in detail. Furthermore, empirical equations to correlate the measured data for the saturated flow boiling heat transfer coefficient, bubble departure diameter, bubble departure frequency, active nucleation site density and boiling heat flux are proposed. The major results obtained here can be summarized and presented as follows:

(1) The boiling incipience is delayed to a higher heat flux at increasing mass flux due to more energy is needed for bubble nucleation. Besides, the micro-pin-fin structures added to the chip can effectively lower the temperature of chip surface in both single-phase and two-phase regions.

(2) The coolant mass flux shows little influence on the saturated flow boiling heat transfer coefficient. Besides, increasing the imposed heat flux significantly promotes boiling heat transfer. Moreover, addition of micro-pin-fins is also beneficial to enhance single-phase and two-phase boiling heat transfer coefficients.

(3) The mean bubble departure diameter is reduced at increasing mass flux. Besides, the higher imposed heat flux results in a larger bubble departure diameter but the smaller mean bubble departure diameter is found on the pin-finned surfaces due to the partial acceleration effect when the coolant passes through the space between two adjacent fins.

(4) Bubble departure frequency increases as the coolant mass flux and imposed heat flux increase. Besides, higher bubble departure frequency is found on the pin-finned surfaces.

(5) Active nucleation site density decreases at increasing coolant mass flux. However, an opposite trend results for an increase in the imposed heat flux and the addition of the micro-pin-fin structures to the chip surface.

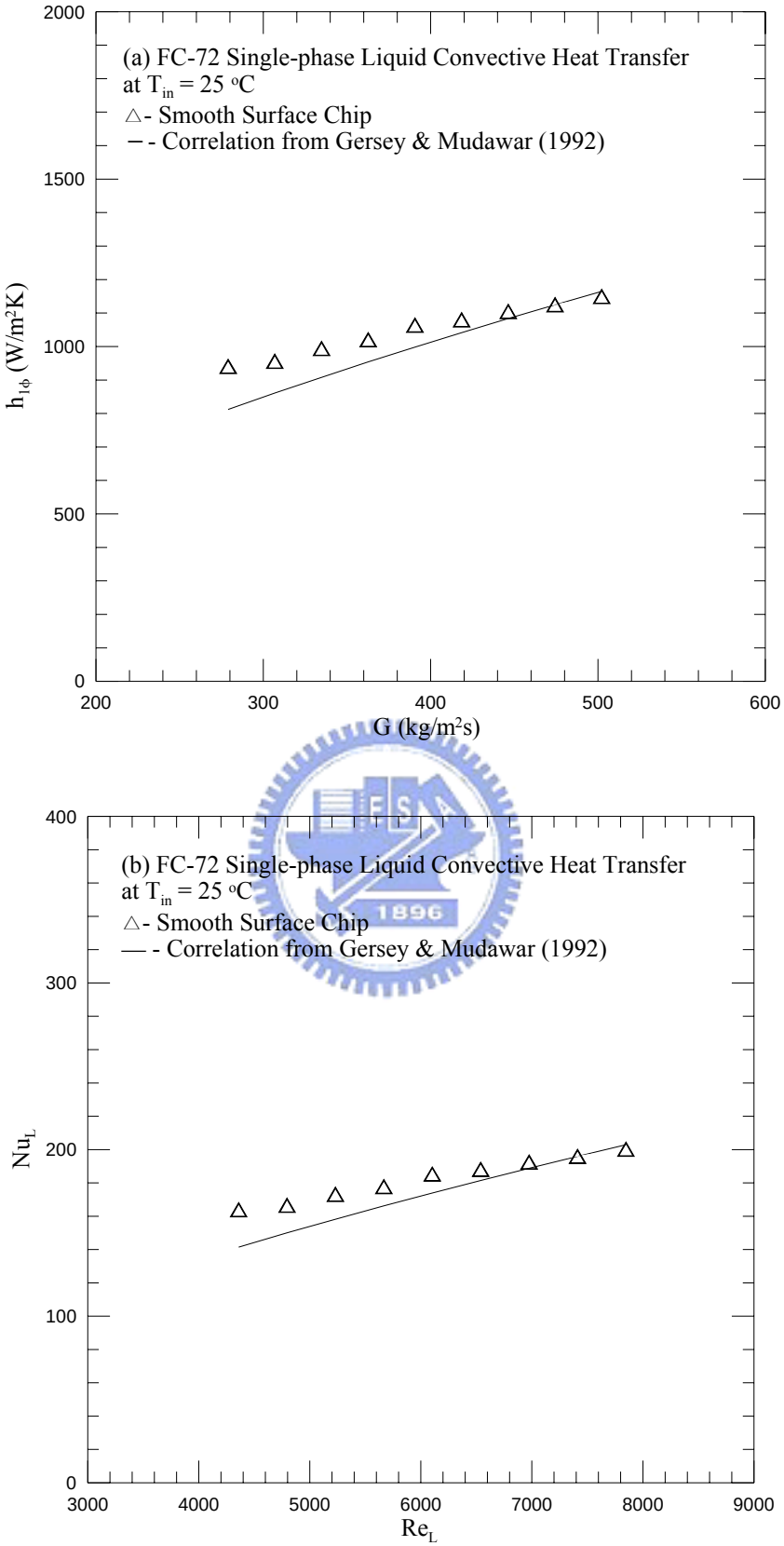

Fig. 4.1 Comparison of the present single-phase liquid convection heat transfer data for the chip with a smooth surface with the correlation of Gersey and Mudawar (1992) for (a) $h_{1\phi}$ vs. G and (b) Nu_L vs. Re_L

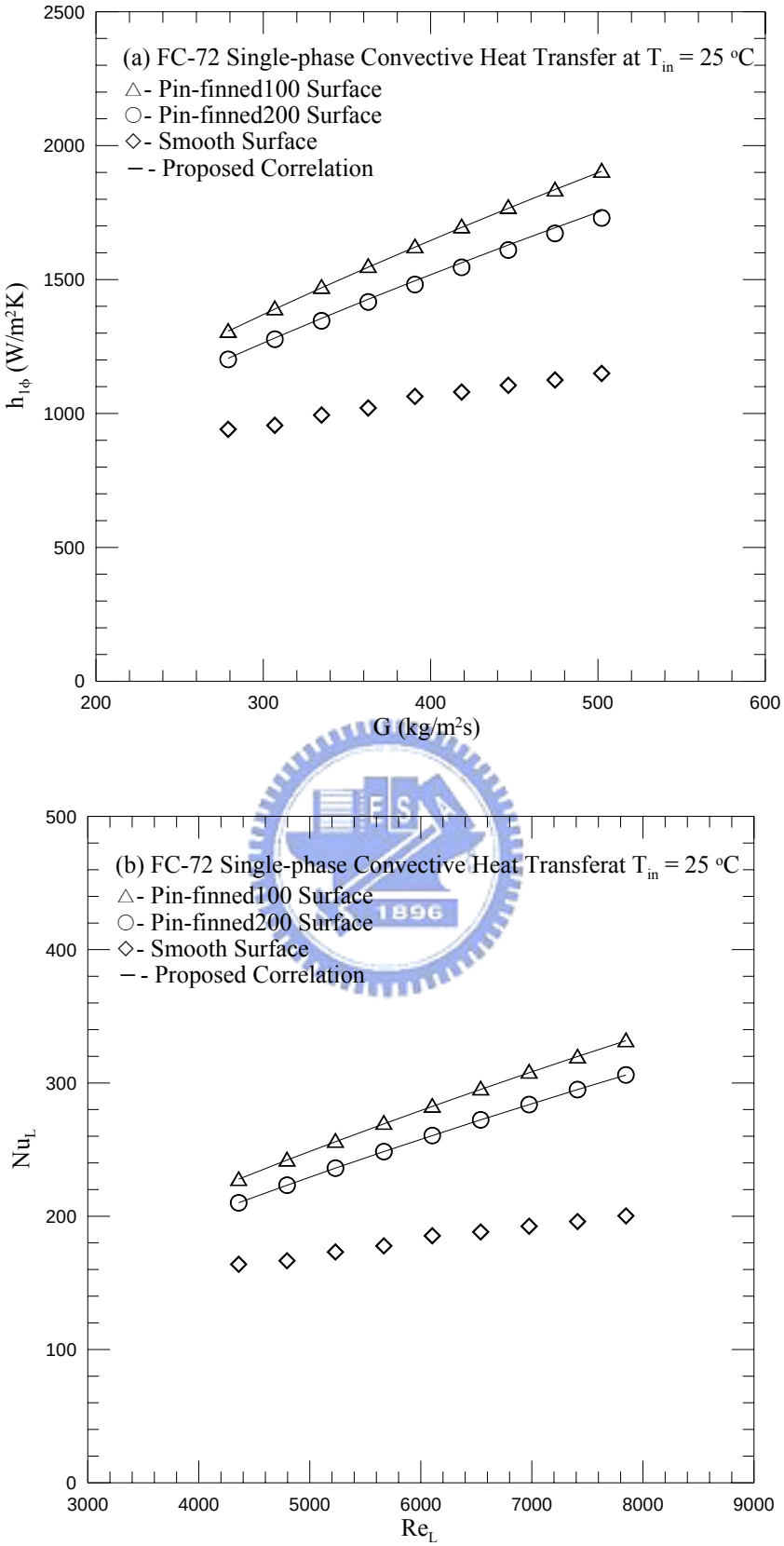

Fig. 4.2 Effects of the micro pin-fins on single-phase liquid convective heat transfer coefficients at T_{in} = 25 °C for (a) $h_{1\phi}$ vs. G and (b) Nu_L vs. Re_L

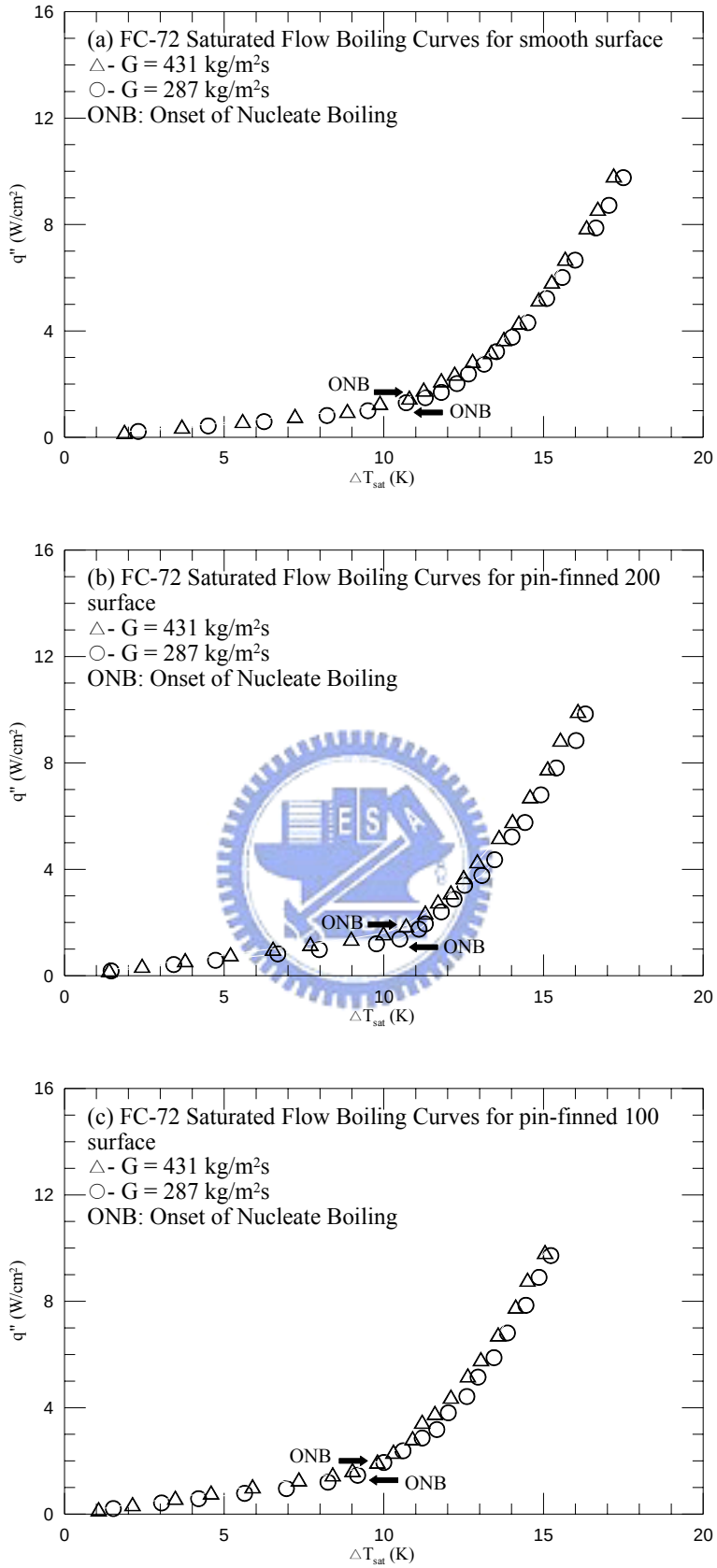

Fig. 4.3 Boiling curves for various coolant mass fluxes for T_{sat} = 54.3 ^{o}C for the chip with (a) smooth surface and (b) pin-finned 200 surface and (c) pin-finned 100 surface

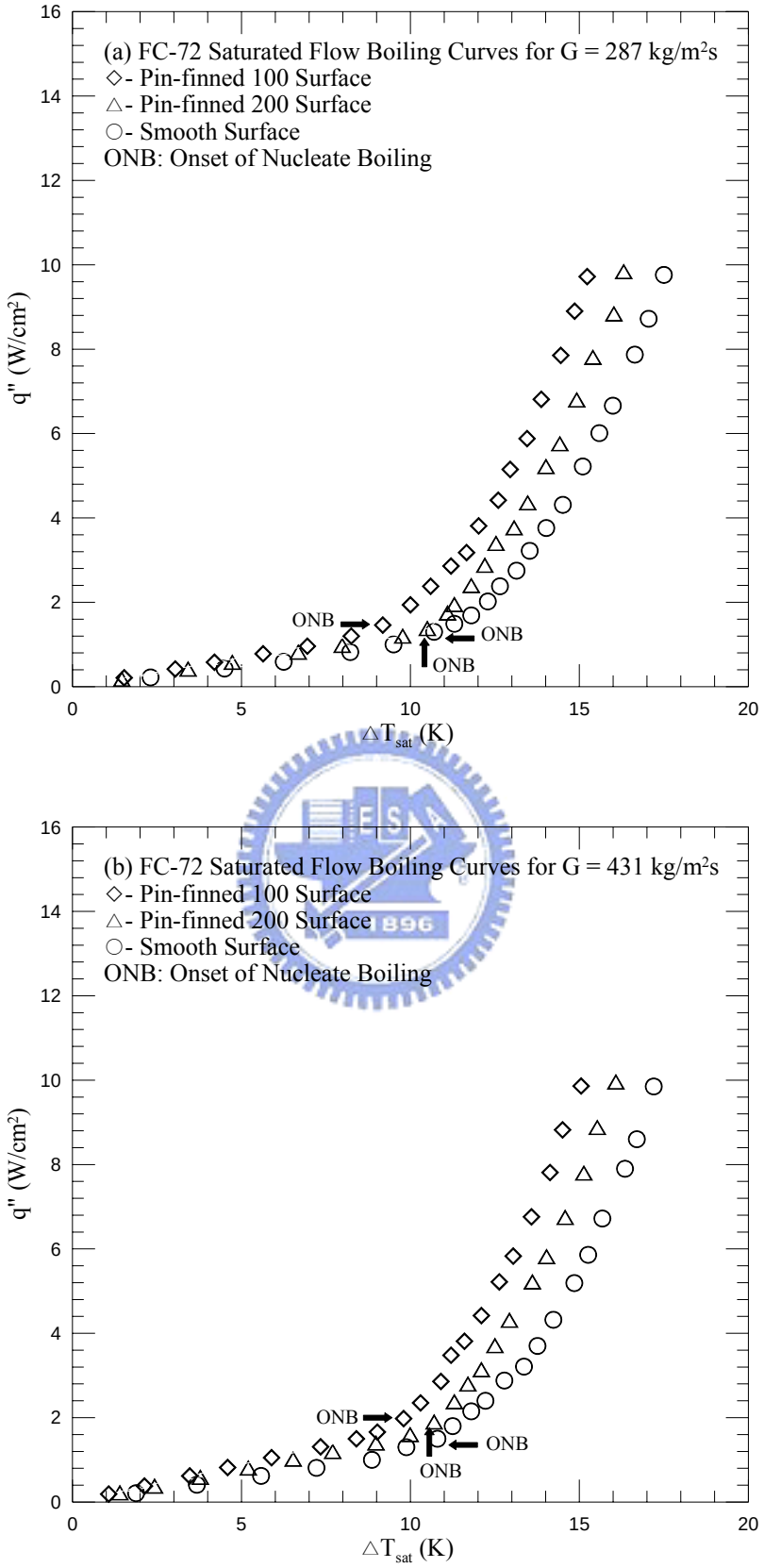

Fig. 4.4 Boiling curves for various micro-structures of chip surface for T_{sat} = 54.3 ^{o}C at (a) G = 287 kg/m^{2}s and (b) G = 431 kg/m^{2}s

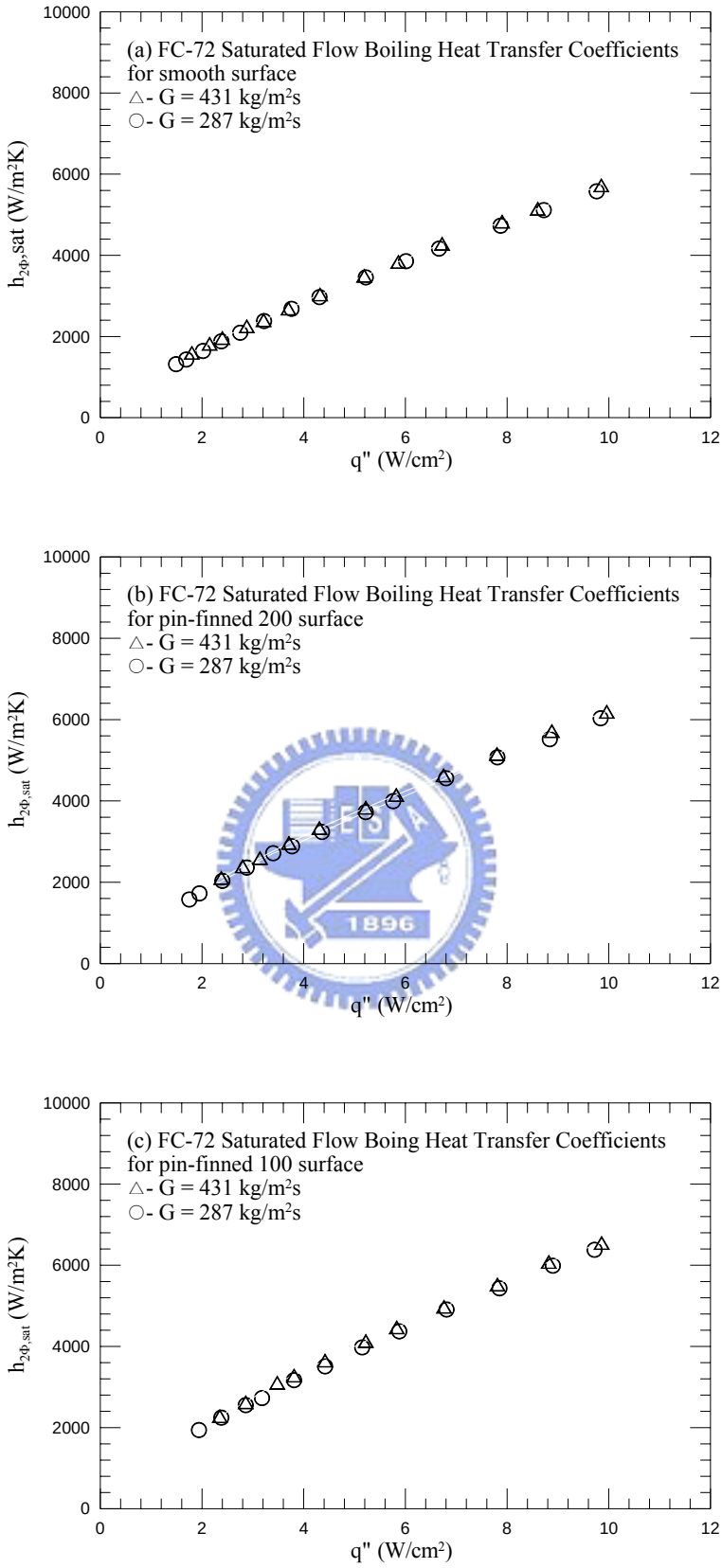

Fig. 4.5 Saturated flow boiling heat transfer coefficients for various coolant mass fluxes for T_{sat} = 54.3 ^{o}C for the chip with (a) smooth surface and (b) pin-finned 200 surface and (c) pin-finned 100 surface

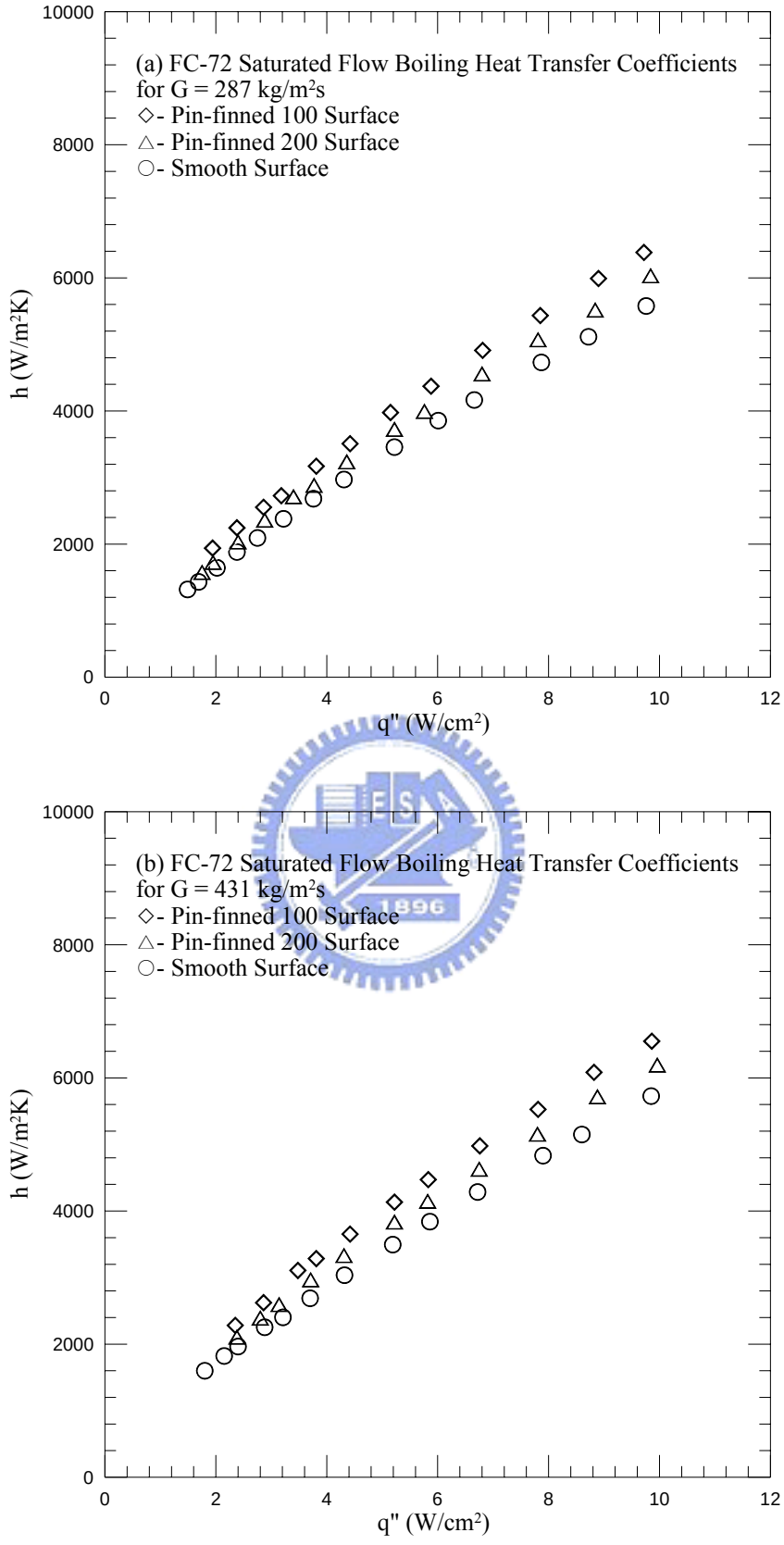

Fig. 4.6 Saturated flow boiling heat transfer coefficients for various micro-structures of chip surface for T_{sat} = 54.3 ^{o}C at (a) G = 287 kg/m^{2}s and (b) G = 431 kg/m^{2}s

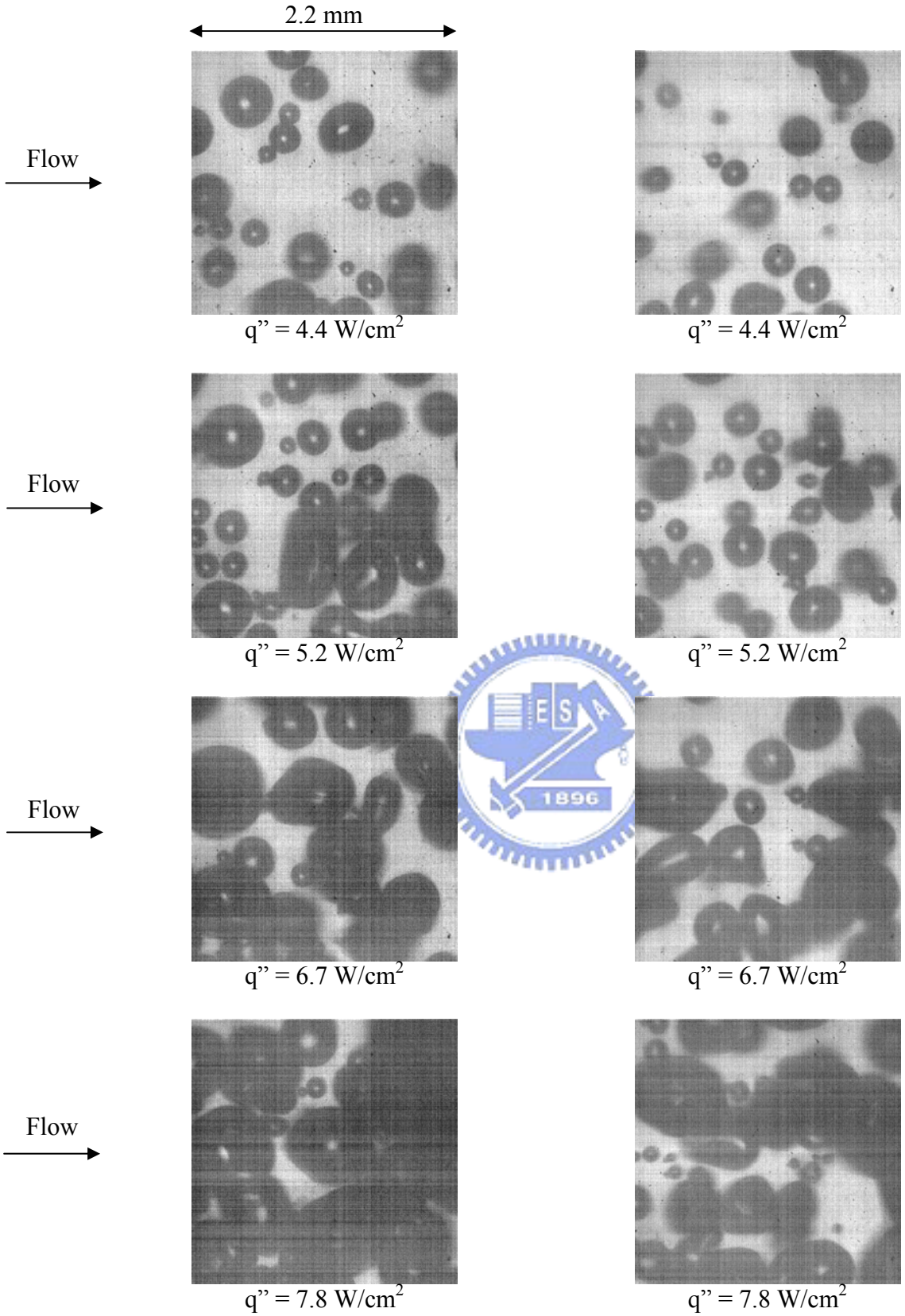

Fig. 4.7 Photos of boiling flow for various imposed heat fluxes for chip with smooth surface for (a) G = 287 kg/m^{2}s and (b) G = 431 kg/m^{2}s

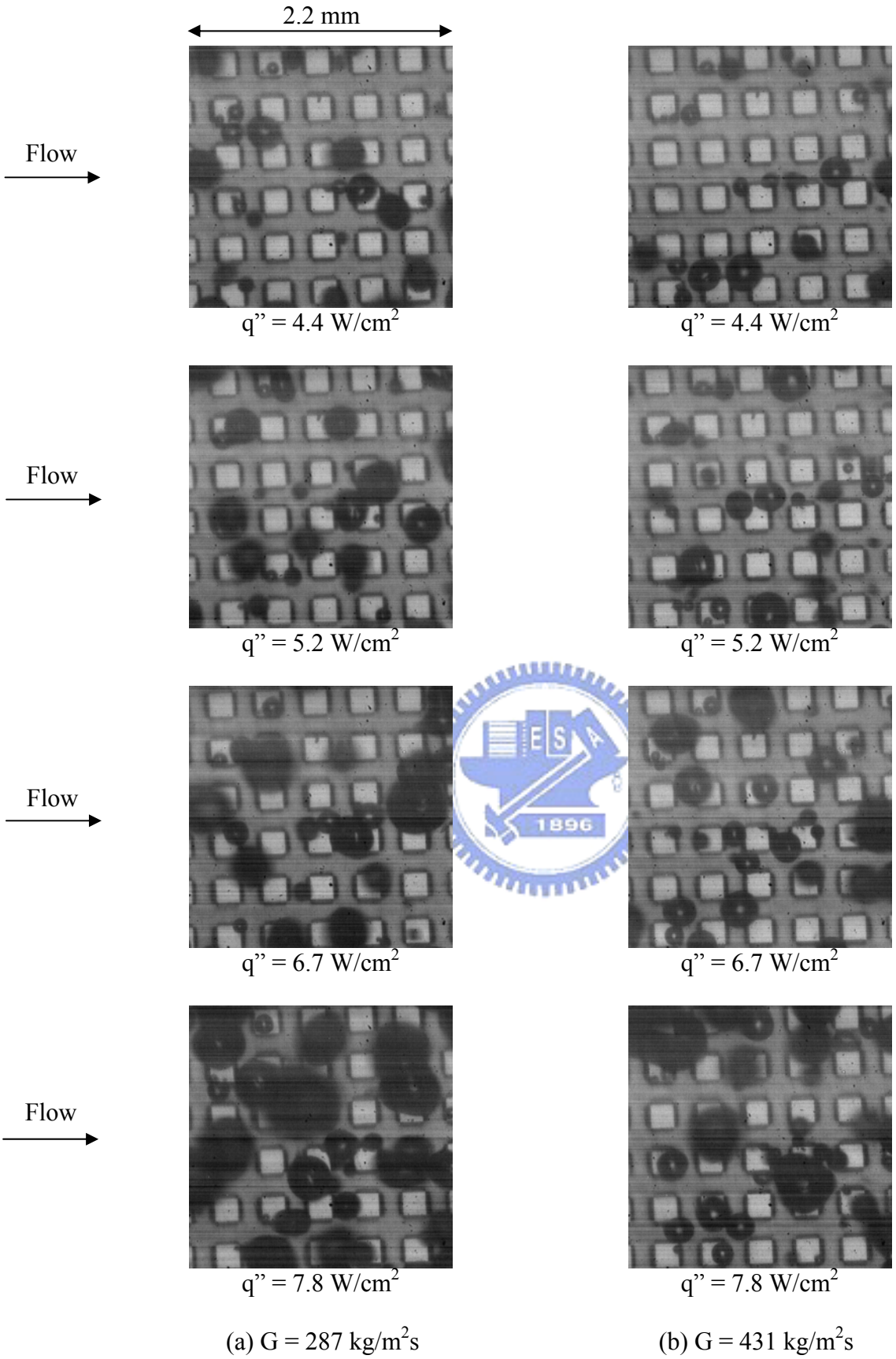

Fig. 4.8 Photos of boiling flow for various imposed heat fluxes for chip with pin-finned 200 surface for (a) G = 287 kg/m^{2}s and (b) G = 431 kg/m^{2}s

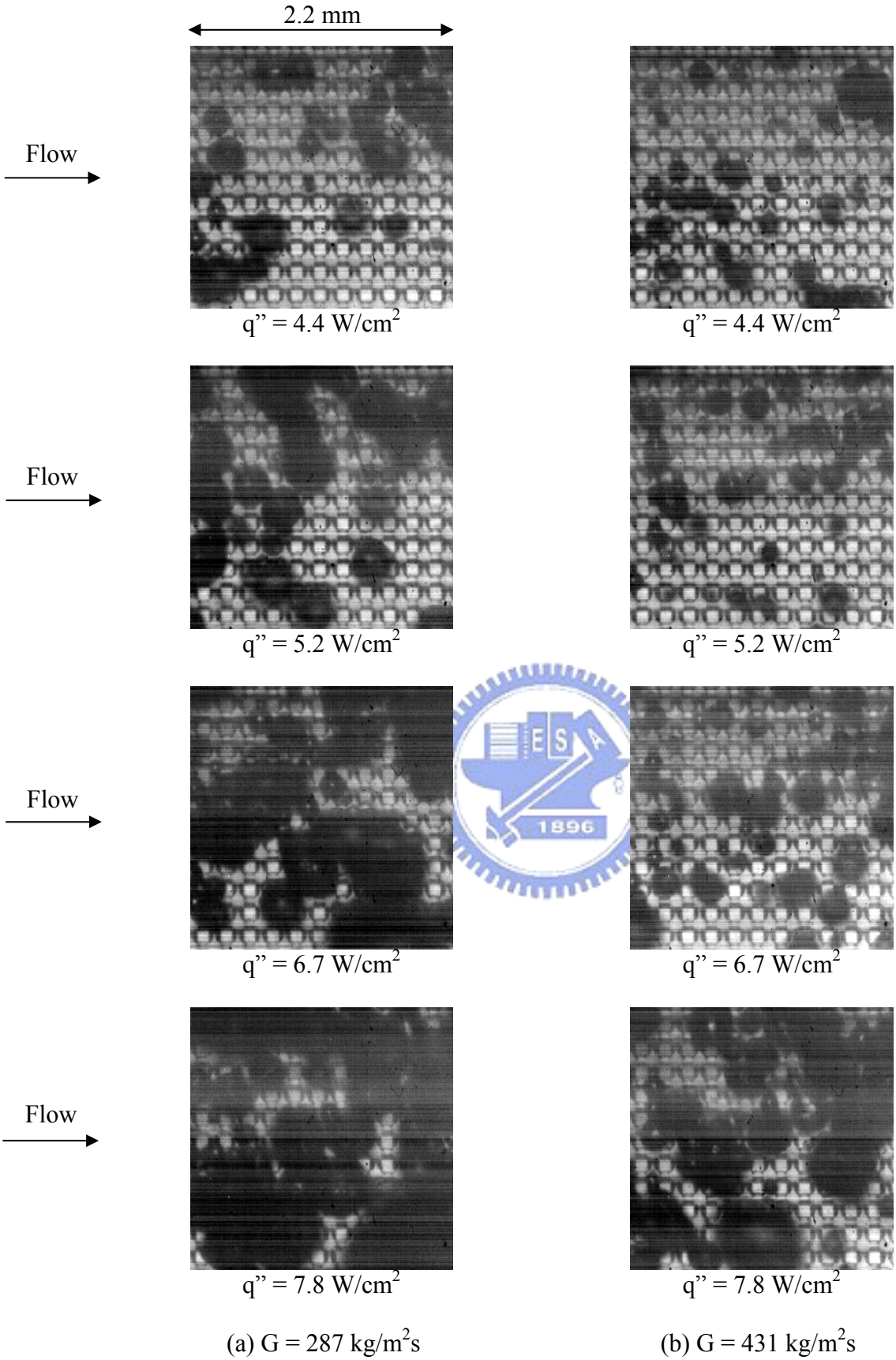

Fig. 4.9 Photos of boiling flow for various imposed heat fluxes for chip with pin-finned 100 surface for (a) G = 287 kg/m^{2}s and (b) G = 431 kg/m^{2}s

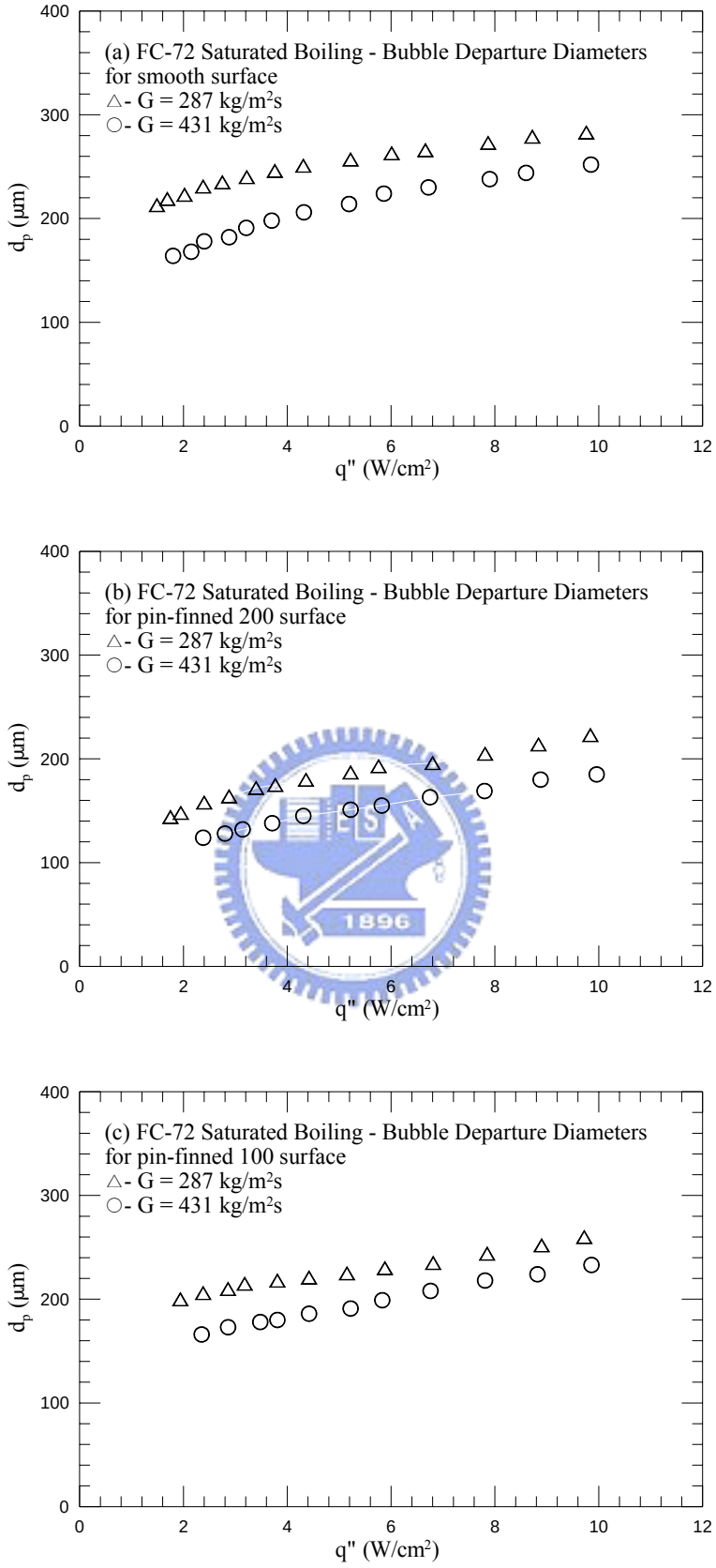

Fig. 4.10 Mean bubble departure diameters for various coolant mass fluxes for T_{sat} = 54.3 ^{o}C for the chip with (a) smooth surface and (b) pin-finned 200 surface and (c) pin-finned 100 Surface

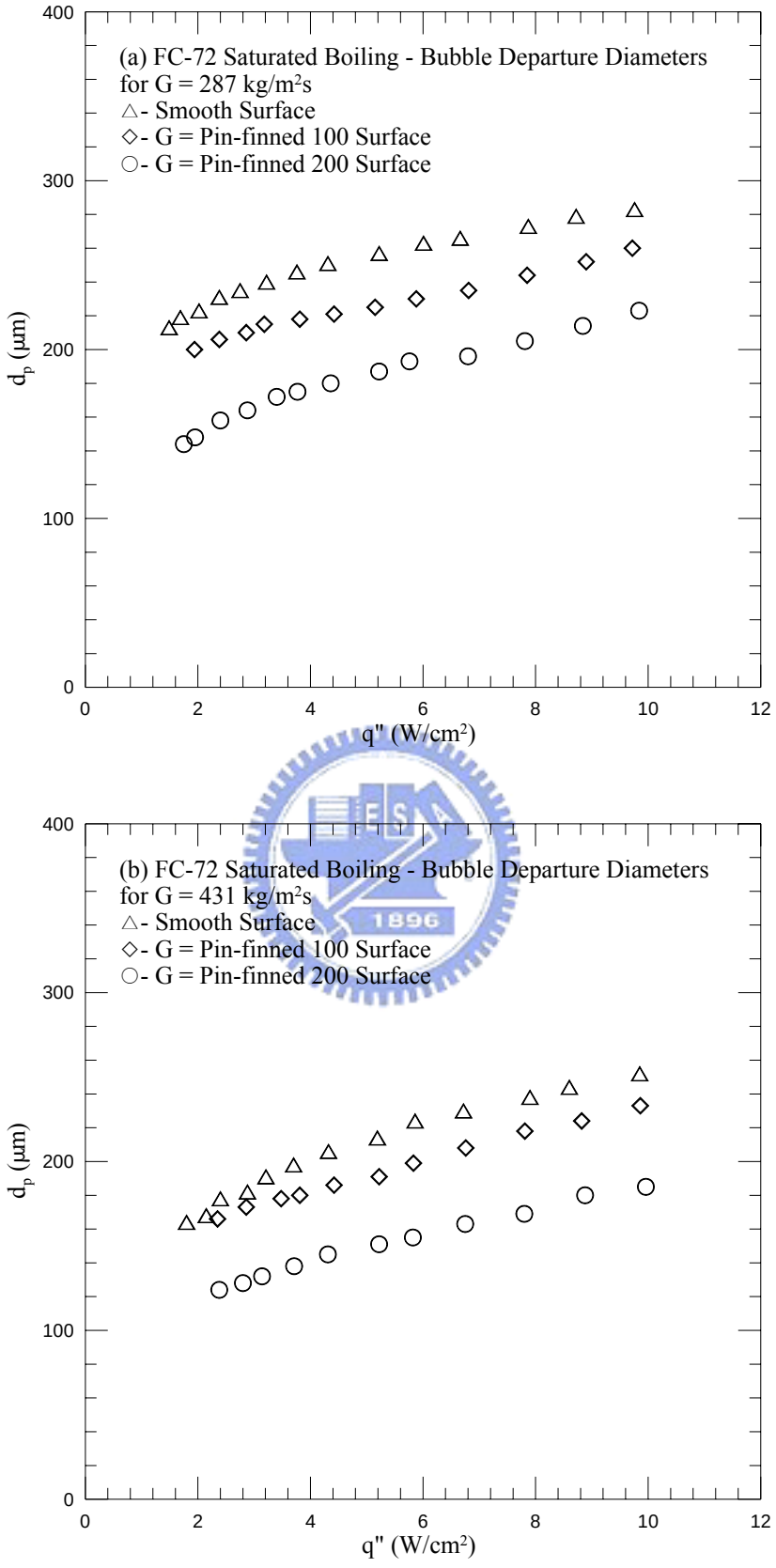

Fig. 4.11 Mean bubble departure diameters for various micro-structures of chip surface for T_{sat} = 54.3 ^{o}C at (a) G = 287 kg/m^{2}s and (b) G = 431 kg/m^{2}s

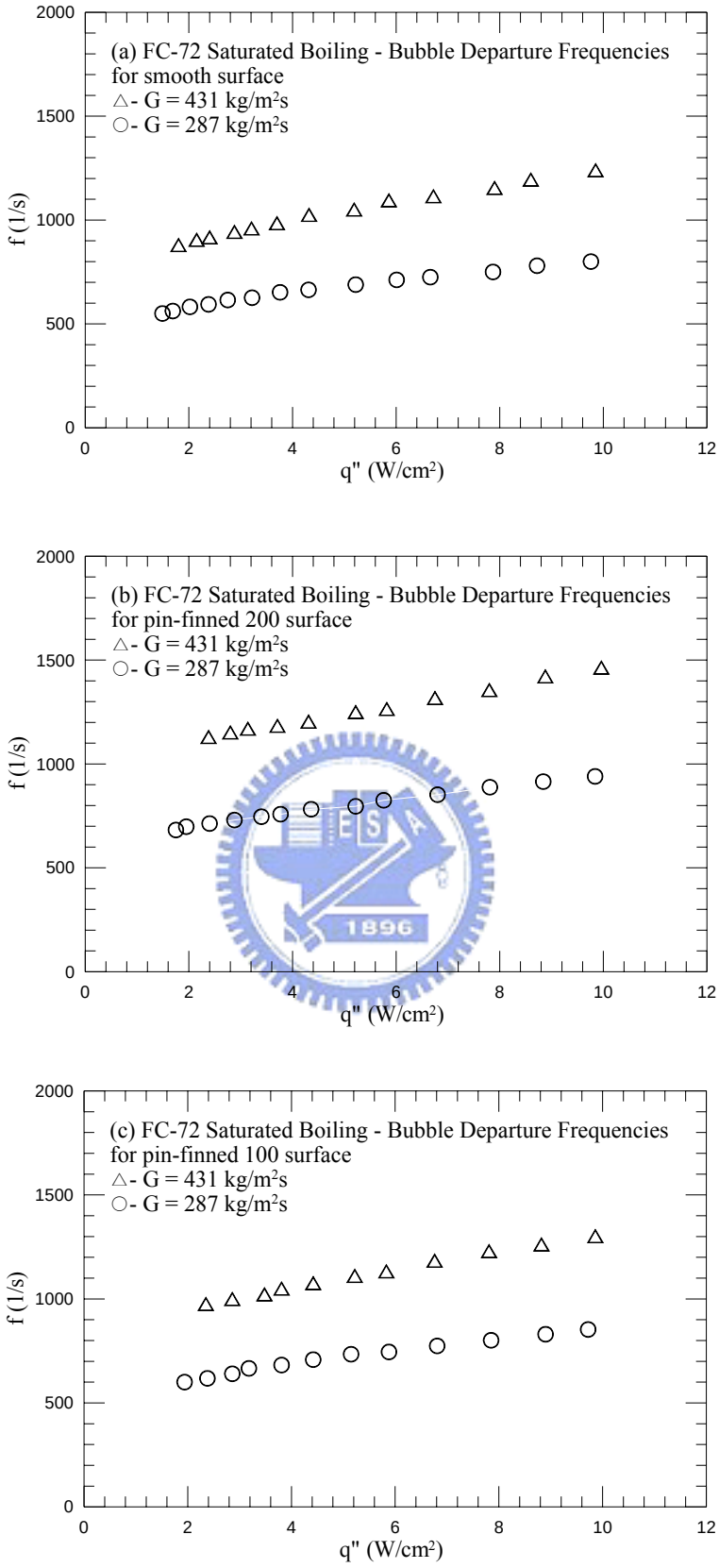

Fig. 4.12 Mean bubble departure frequencies for various coolant mass fluxes for T_{sat} = 54.3 ^{o}C for the chip with (a) smooth surface and (b) pin-finned 200 Surface and (c) pin-finned 100 surface

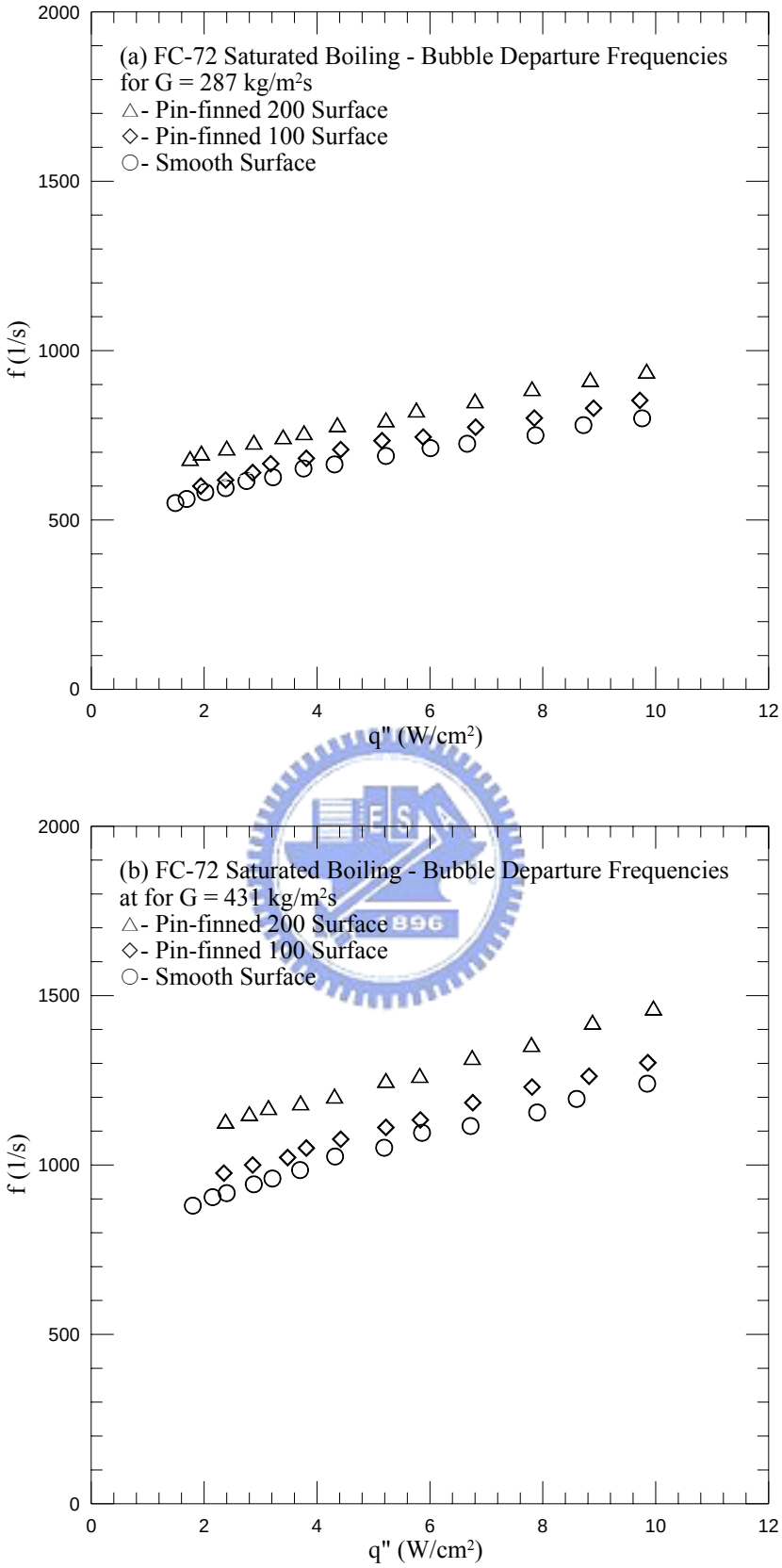

Fig. 4.13 Mean bubble departure frequencies for various micro-structures of chip surface for T_{sat} = 54.3 ^{o}C at (a) G = 287 kg/m^{2}s and (b) G = 431 kg/m^{2}s

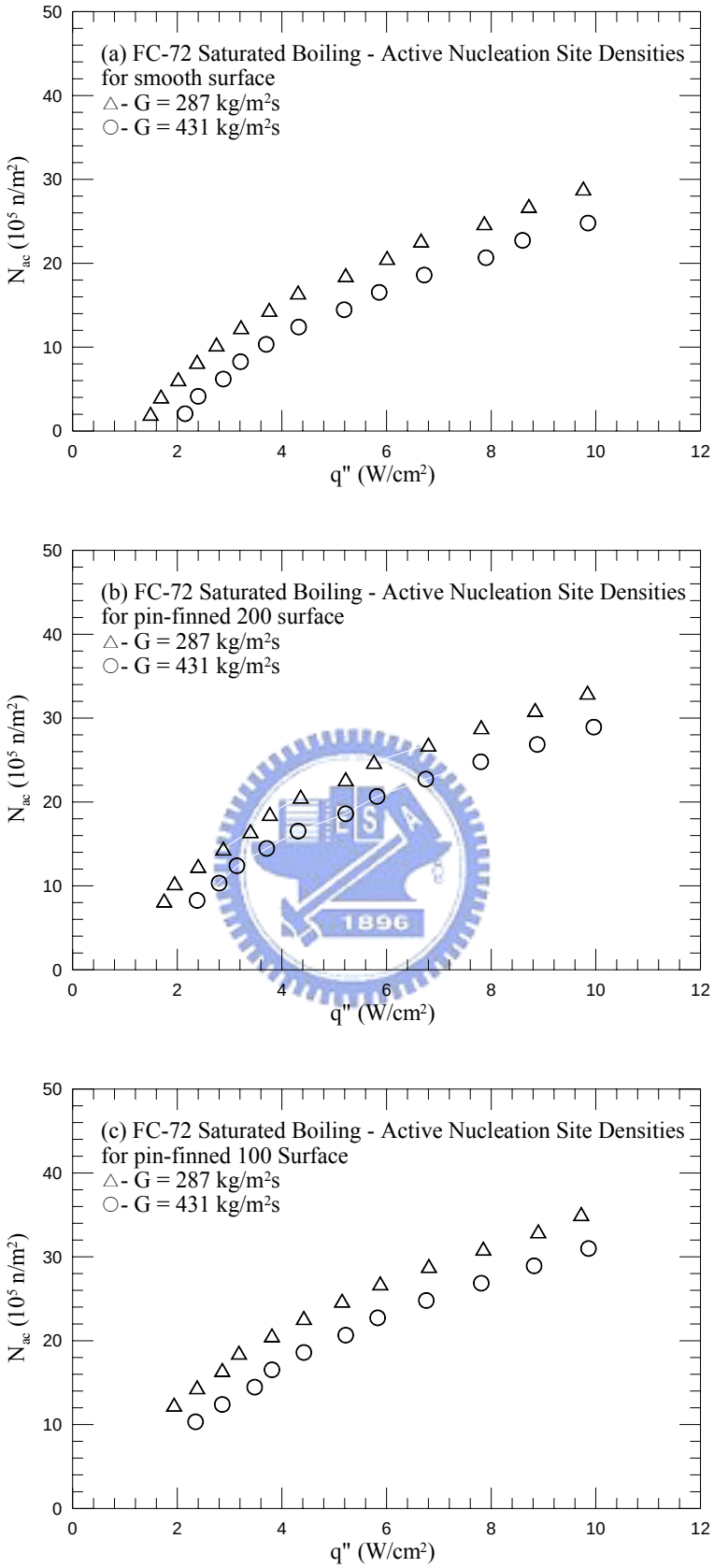

Fig. 4.14 Mean active nucleation site densities for various coolant mass fluxes for T_{sat} = 54.3 ^{o}C for the chip with (a) smooth surface and (b) pin-finned 200 Surface (c) pin-finned 100 Surface

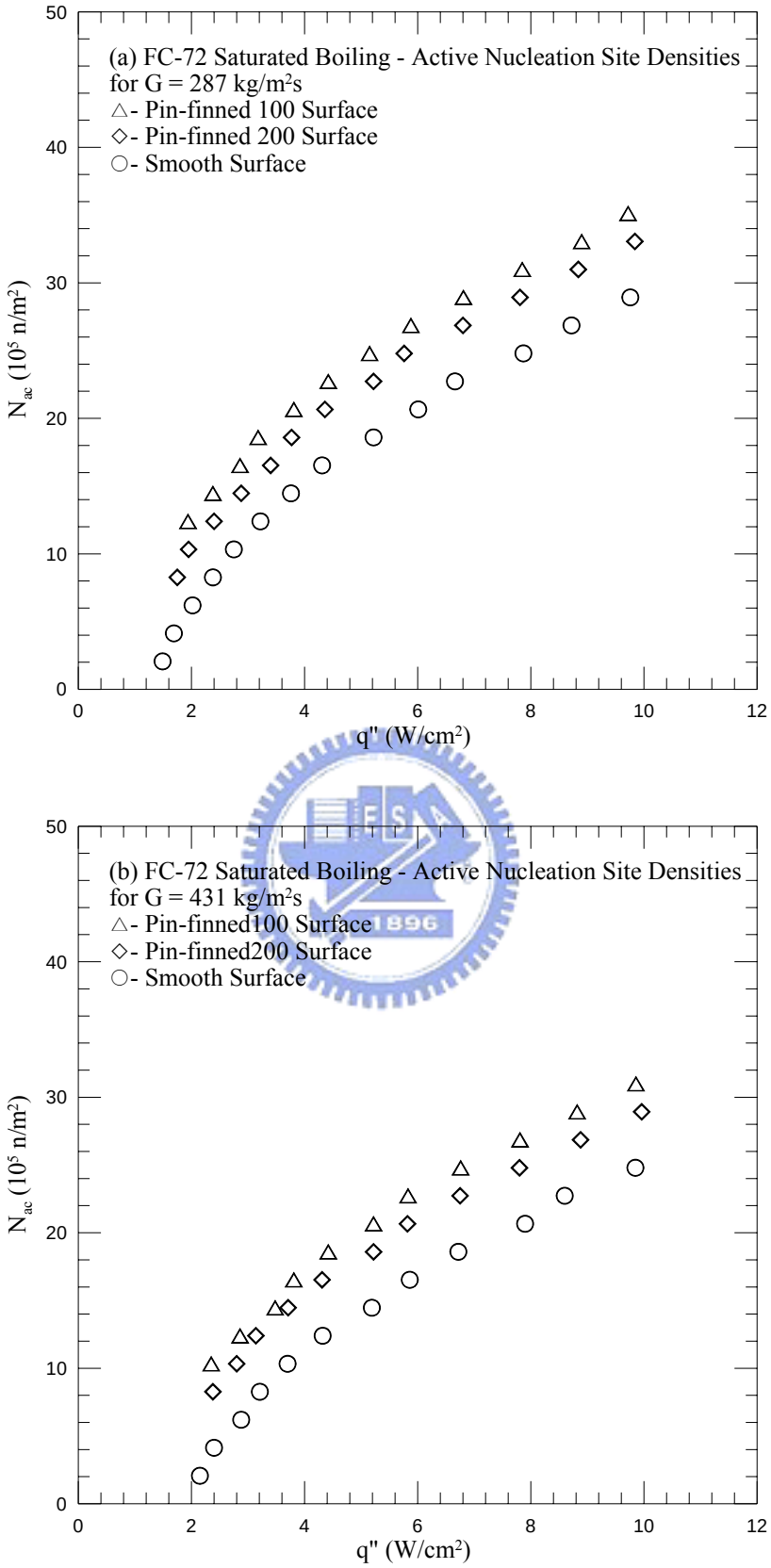

Fig. 4.15 Mean active nucleation site densities for various micro-structures of chip surface for T_{sat} = 54.3 ^{o}C at (a) G = 287 kg/m^{2}s and (b) G = 431 kg/m^{2}s

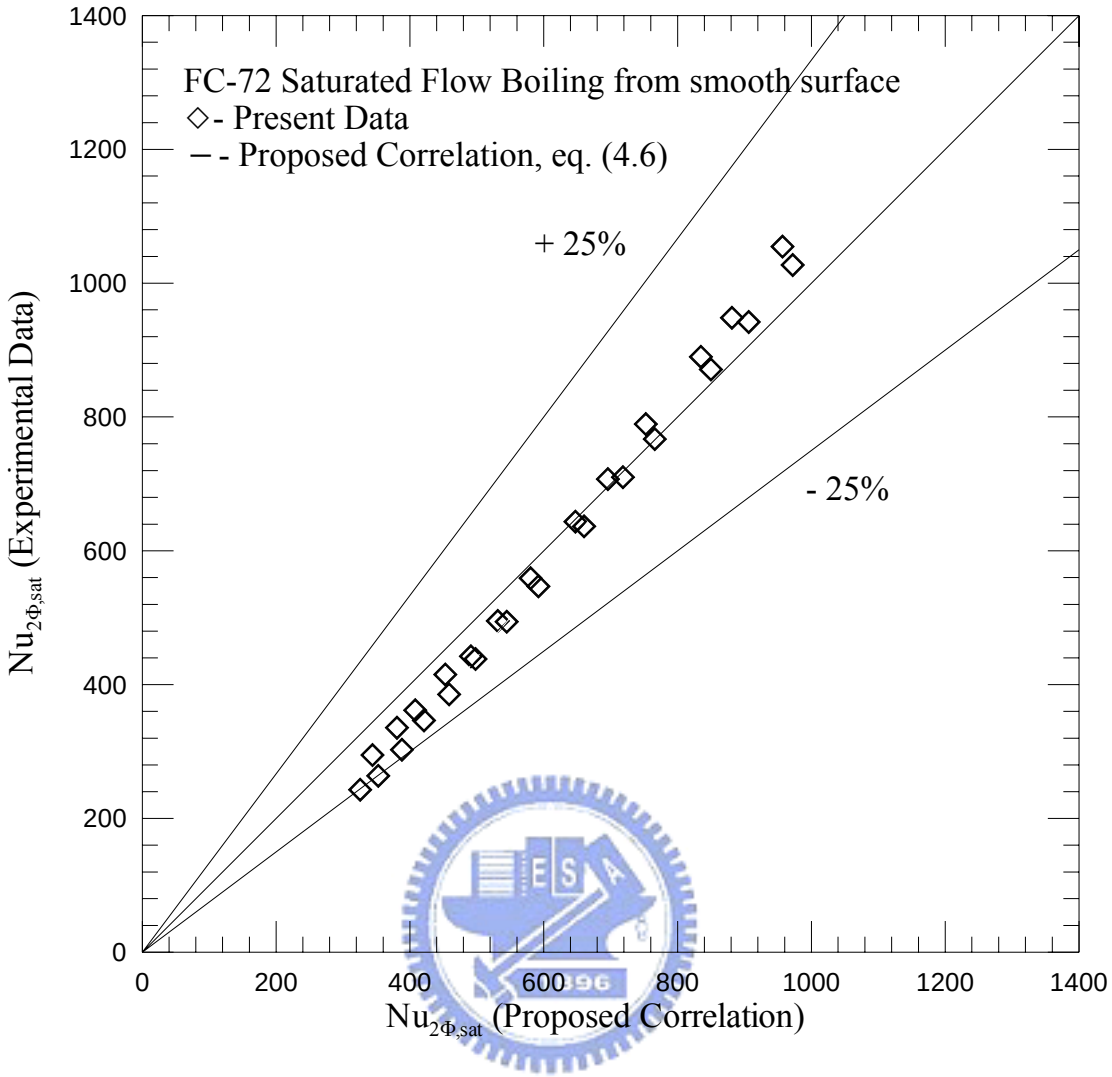

Fig. 4.16 Comparison of the measured data for Nusselt number for saturated flow boiling of FC-72 on smooth surface with the proposed correlation

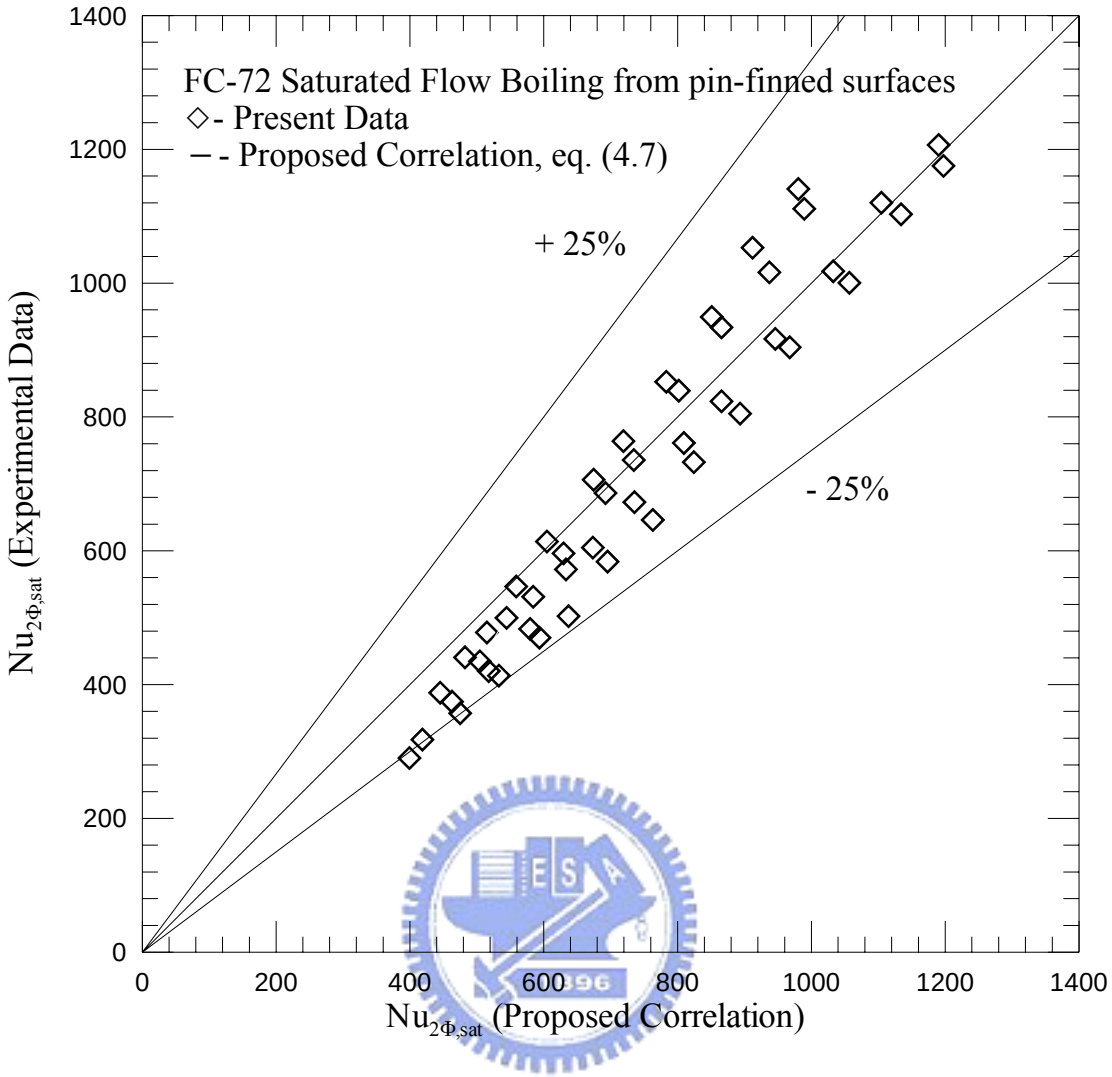

Fig. 4.17 Comparison of the measured data for Nusselt number for saturated flow boiling of FC-72 on pin-finned surfaces with the proposed correlation

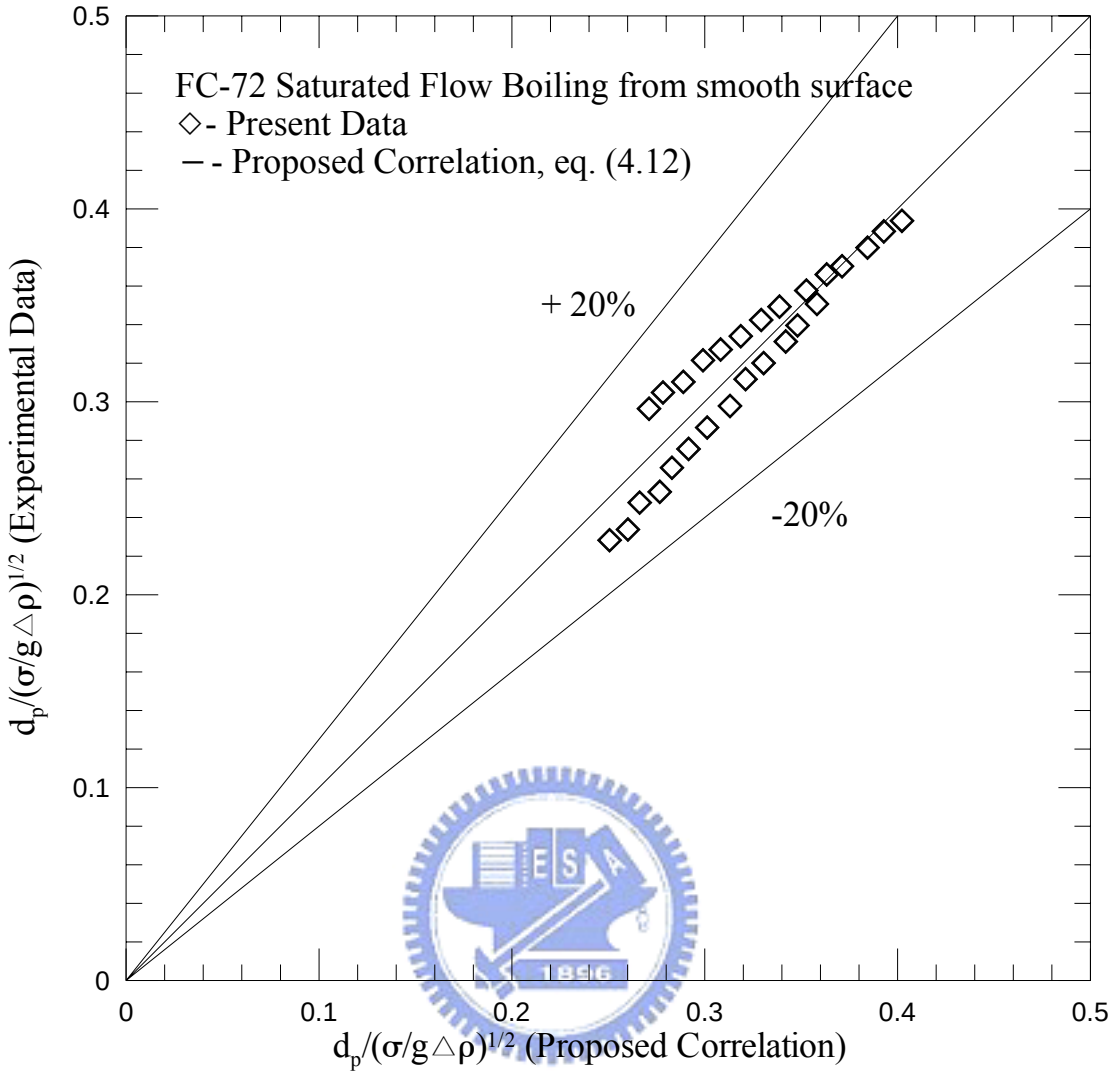

Fig. 4.18 Comparison of the measured data for mean bubble departure diameter for saturated flow boiling of FC-72 on smooth surface with the proposed correlation

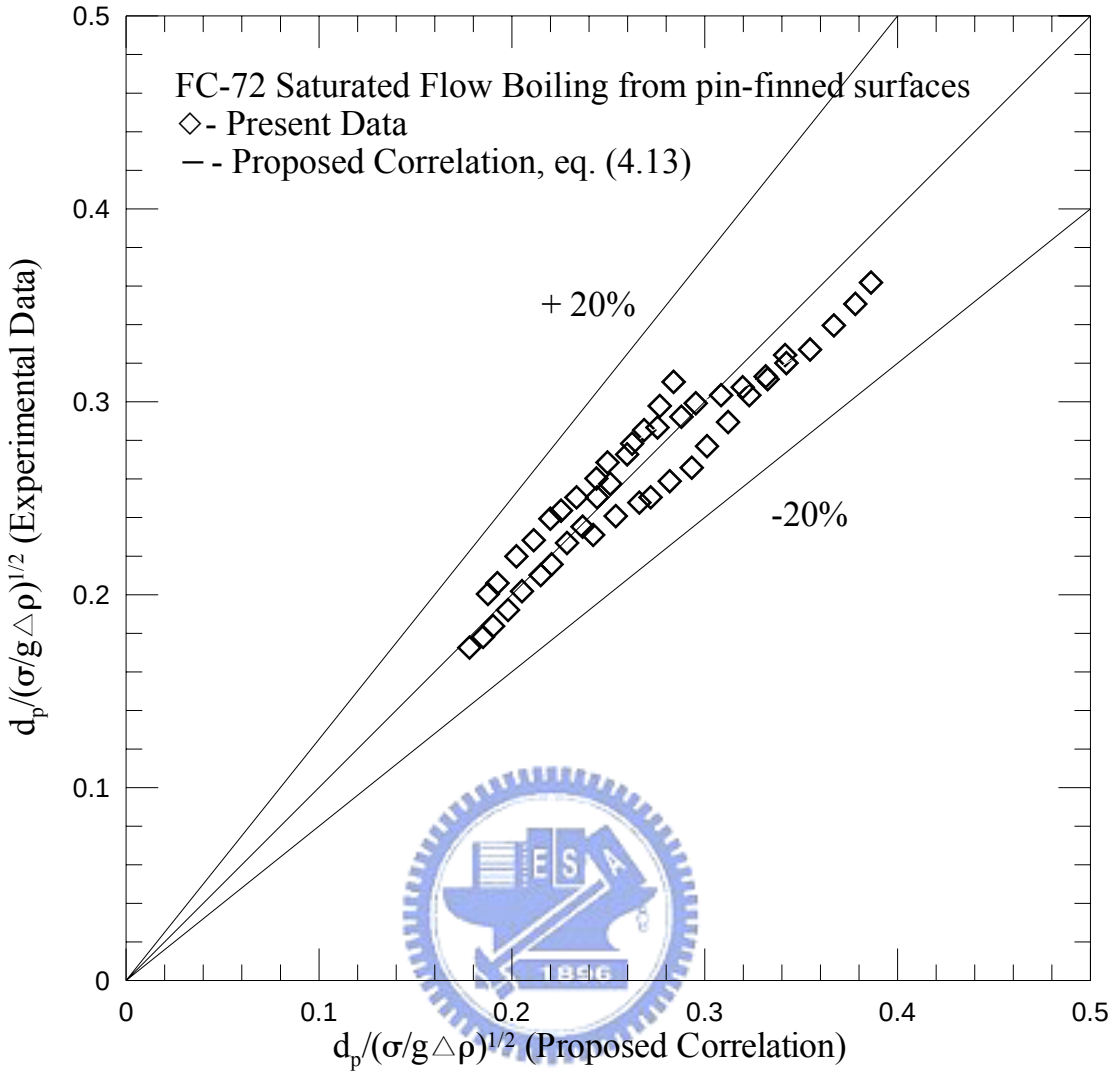

Fig. 4.19 Comparison of the measured data for mean bubble departure diameter for saturated flow boiling of FC-72 on pin-finned surfaces with the proposed correlation

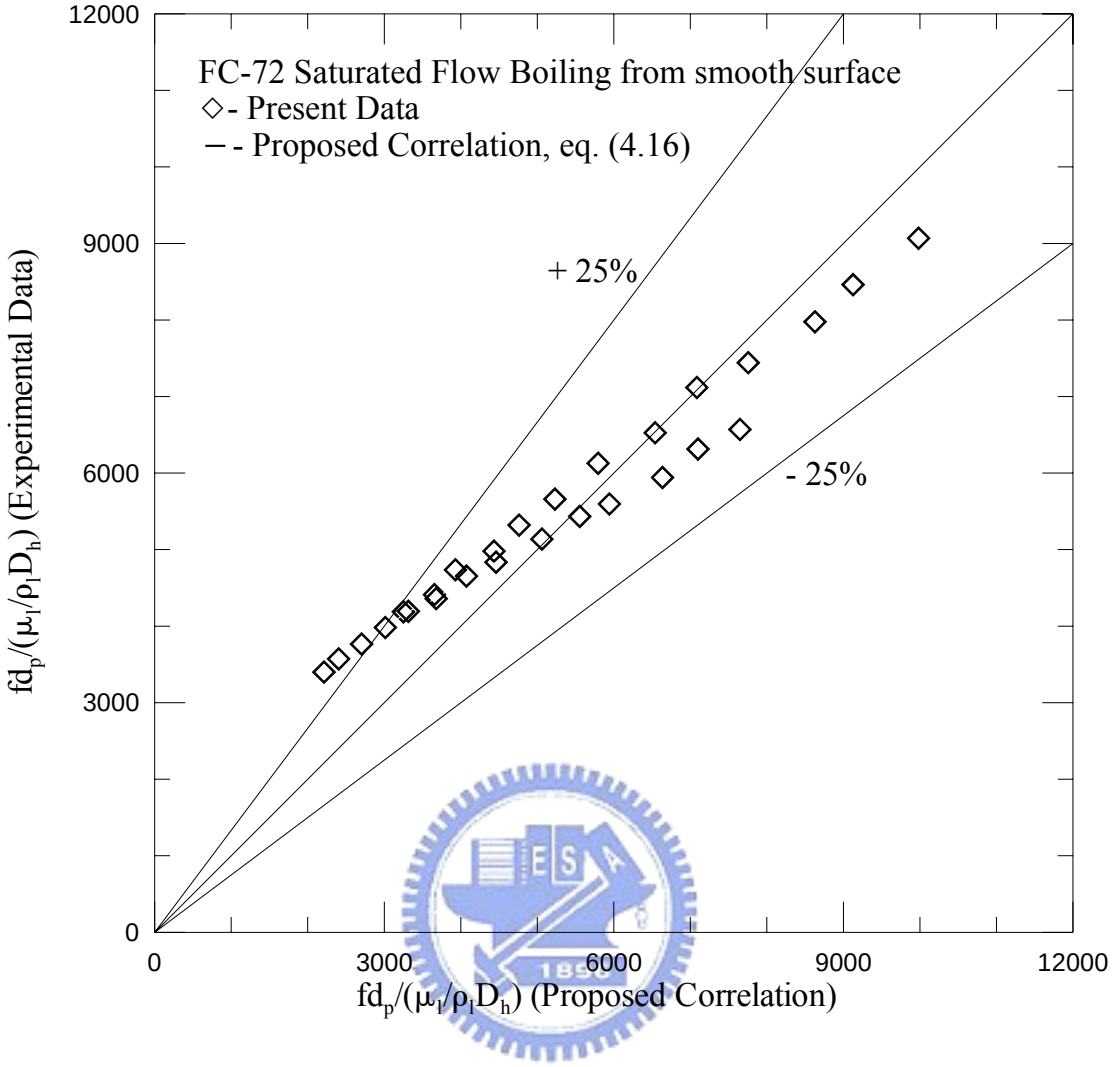

Fig. 4.20 Comparison of the measured data for mean bubble departure frequency for saturated flow boiling of FC-72 on smooth surface with the proposed correlation

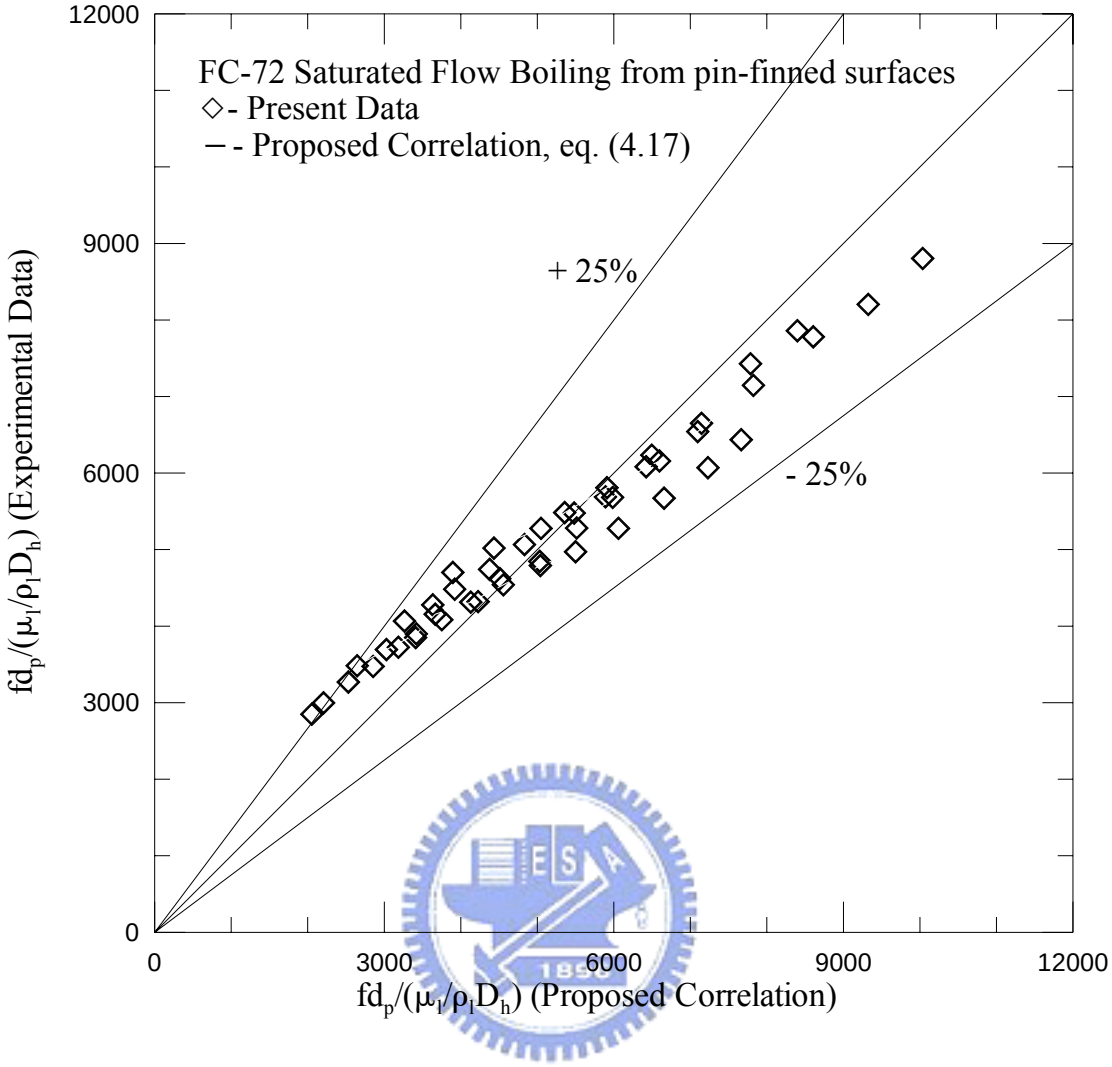

Fig. 4.21 Comparison of the measured data for mean bubble departure frequency for saturated flow boiling of FC-72 on pin-finned surfaces with the proposed correlation

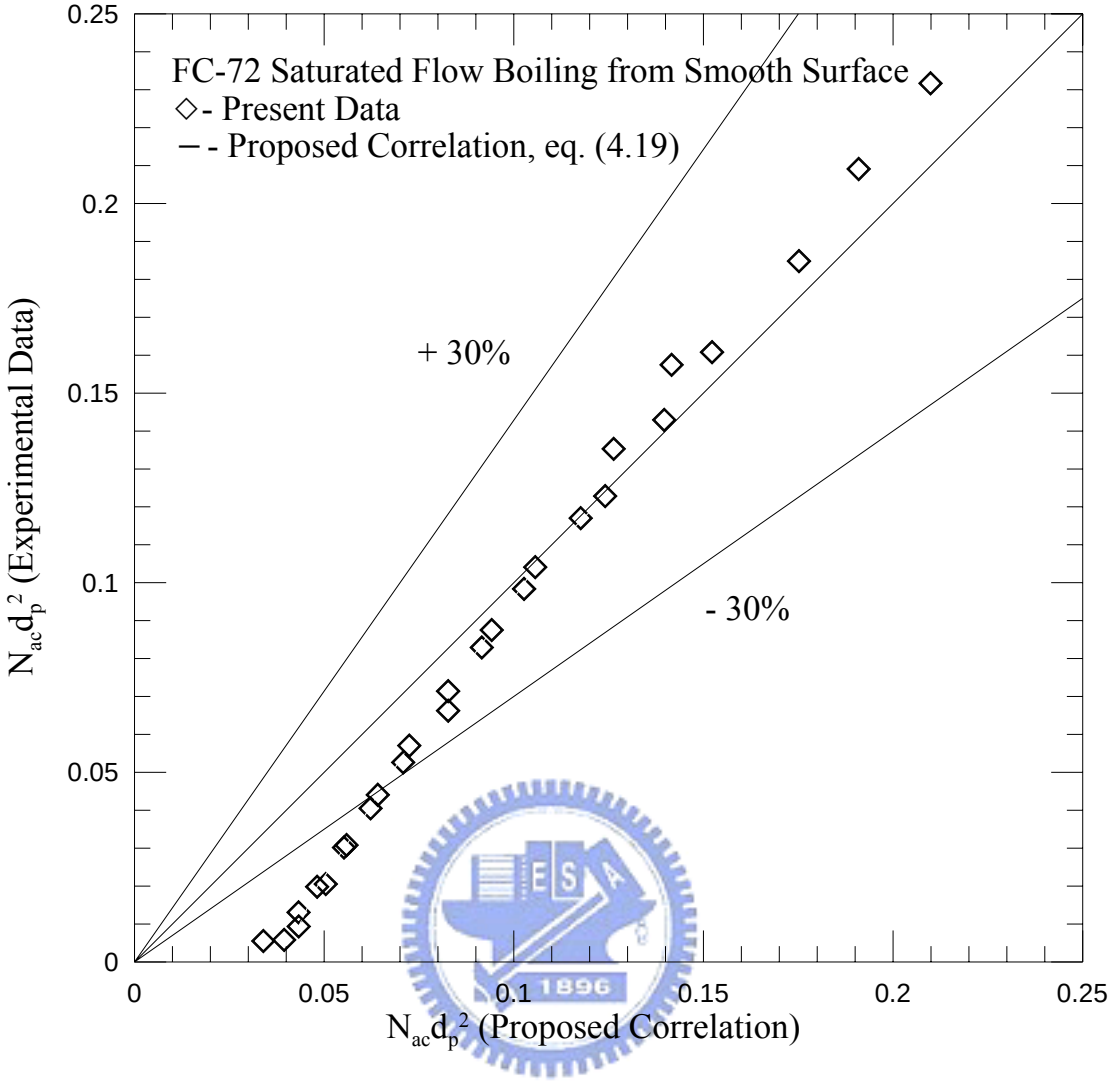

Fig. 4.22 Comparison of the measured data for mean active nucleation site density for saturated flow boiling of FC-72 on smooth surface with the proposed correlation

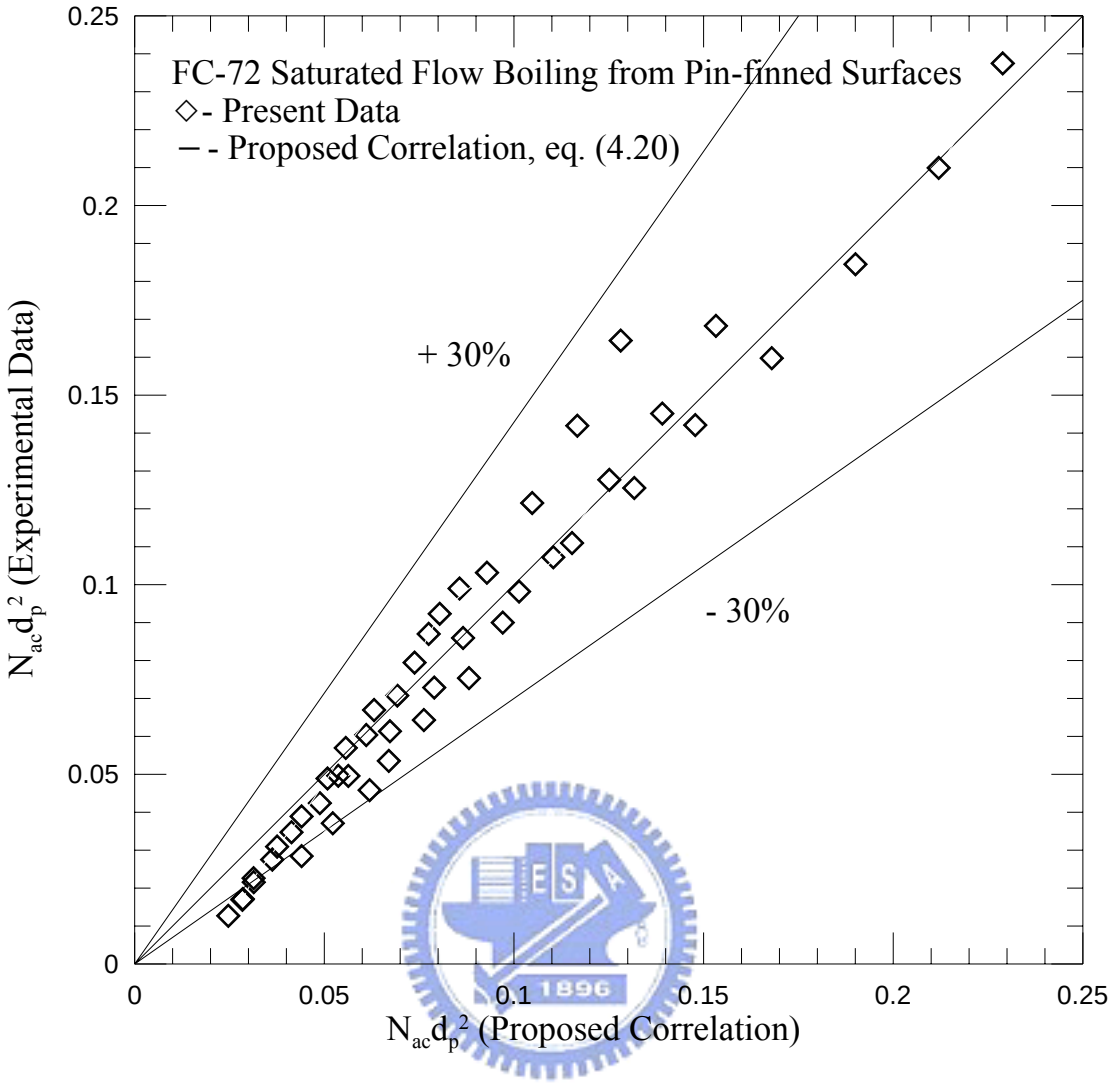

Fig. 4.23 Comparison of the measured data for mean active nucleation site density for saturated flow boiling of FC-72 on pin-finned surfaces with the proposed correlation

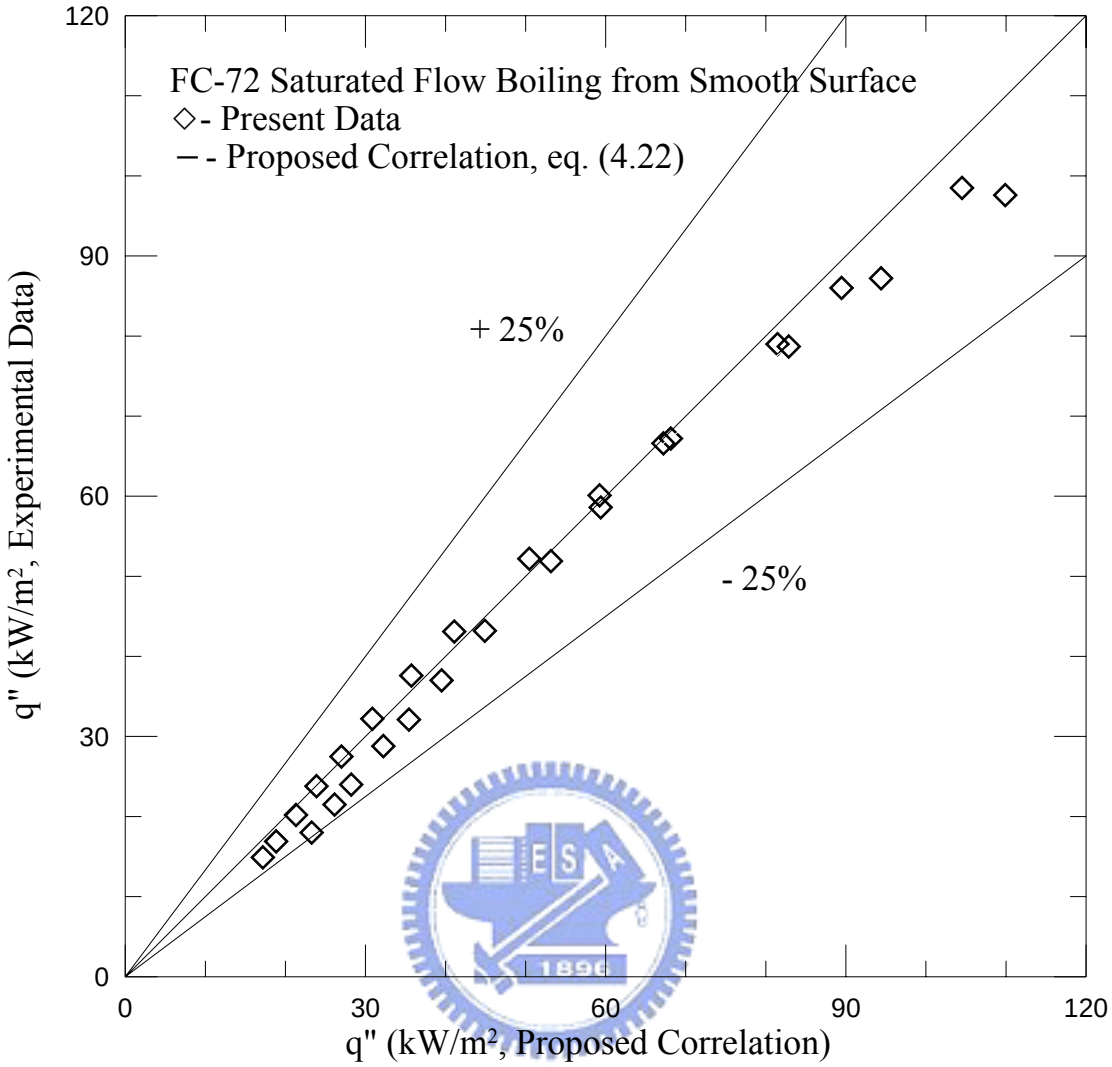

Fig. 4.24 Comparison of the measured data for boiling heat flux for saturated flow boiling of FC-72 on smooth surface with the proposed correlation

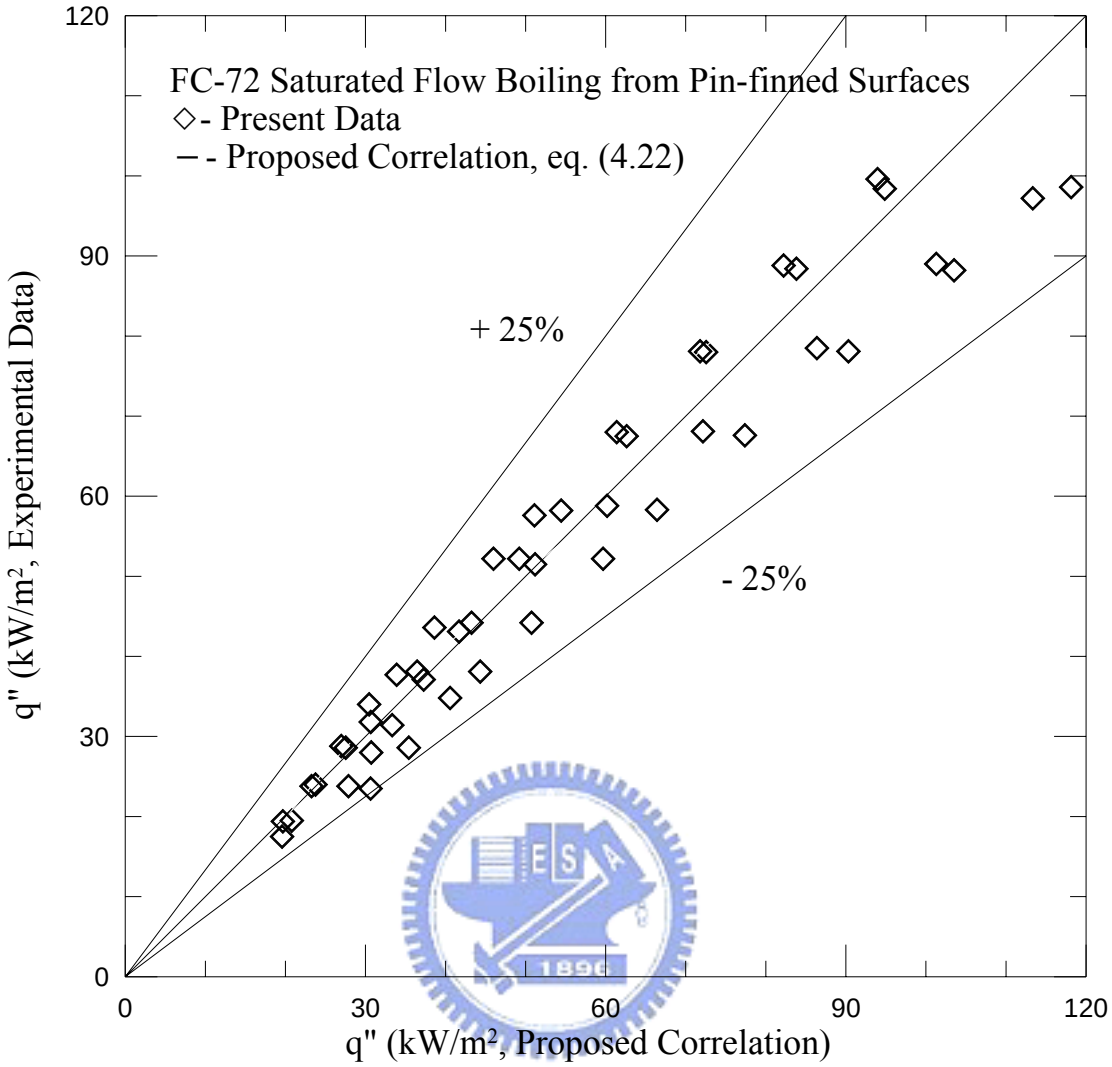

Fig. 4.25 Comparison of the measured data for boiling heat flux for saturated flow boiling of FC-72 on pin-finned surfaces with the proposed correlation